Meteoritics & Planetary Science 38, Nr 2, 197–224 (2003)
Abstract available online at http://meteoritics.org

The petrogenesis of type B1 Ca-Al-rich inclusions: The spinel perspective

Harold C. CONNOLLY Jr.,[1*] D. S. BURNETT,[2] and Kevin D. McKEEGAN[3]

[1]Department of Physical Sciences, Kingsborough College of the City University of New York, 2001 Oriental Blvd., Brooklyn, New York 11235, USA; Department of Earth and Planetary Sciences, American Museum of Natural History, Central Park West, New York, New York 10024, USA; and Department of Geological Sciences, Rutgers University, 610 Taylor Road, Piscataway, New Jersey 08854–8066, USA
[2]Division of Geological and Planetary Sciences, California Institute of Technology, 100–23, Pasadena, California 91125, USA
[3]Department of Earth and Space Sciences, University of California, Los Angeles, California 90095–1567, USA
[*]Corresponding author. E-mail: hconnolly@kbcc.cuny.edu

(Received 12 February 2002; revision accepted 17 February 2003)

Abstract–Minor element variations in $MgAl_2O_4$ spinel from the type B1 calcium-aluminum-rich inclusion (CAI) Allende TS-34 confirm earlier studies in showing correlations between the minor element chemistry of spinels with their location within the inclusion and with the chemistry of host silicate phases. These correlations result from a combination of crystallization of a liquid produced by re-melting event(s) and local re-equilibration during subsolidus reheating. The correlation of the Ti and V in spinel inclusions with the Ti and V in the adjacent host clinopyroxene can be qualitatively explained by spinel and clinopyroxene crystallization prior to melilite, following a partial melting event. There are, however, difficulties in quantitative modeling of the observed trends, and it is easier to explain the Ti correlation in terms of complete re-equilibration. The correlation of V in spinel inclusions with that in the adjacent host clinopyroxene also cannot be quantitatively modeled by fractional crystallization of the liquid produced by re-melting, but it can be explained by partial re-equilibration. The distinct V and Ti concentrations in spinel inclusions in melilite from the edge regions of the CAI are best explained as being affected by only a minor degree of re-equilibration. The center melilites and included spinels formed during crystallization of the liquid produced by re-melting, while the edge melilites and included spinels are primary. The oxygen isotope compositions of TS-34 spinels are uniformly ^{16}O-rich, regardless of the host silicate phase or its location within the inclusion. Similar to other type B1 CAIs, clinopyroxene is ^{16}O-rich, but melilite is relatively ^{16}O-poor. These data require that the oxygen isotope exchange in TS-34 melilite occurred subsequent to the last re-melting event.

INTRODUCTION

Type B calcium-aluminum-rich inclusions (CAIs) were among the first igneous rocks produced within our solar system. These cm-sized spheres, which are found only in CV3 carbonaceous chondrites, have been the focus of much research (see MacPherson, Wark, and Armstrong 1988). Until a few years ago, the study of these early planetary materials was dominated by the concept that they had experienced a simple, single-stage igneous crystallization history, with oxygen isotope exchange occurring within all inclusions and post-solidification alteration occurring in many of them. However, an increasing amount of evidence points to an unavoidable conclusion: type B CAIs have experienced multiple partial-melting events (MacPherson and Davis 1993; Davis and MacPherson 1996; Davis, Simon, and Grossman 1998; Connolly and Burnett 1999; Beckett, Simon, and Stolper 2000; Yurimoto, Ito, and Nagasawa 1998). One of the most important constraints on the mechanism that produced Fe, Mg-rich chondrules is that it is required to have been repeatable and provide a means for the same chondrule to experience different degrees of reheating (Connolly and Love 1997; Jones et al. 2002). Thus, the same constraint can be applied to the mechanism(s) that produced type B CAIs, whether it was the same or different from the one that produced Fe, Mg-rich chondrules.

We previously inferred the existence of multiple melting events from a study of spinel minor element compositions in two type B CAIs (Connolly and Burnett 1999). Here, we test the previously-drawn conclusions by extending our studies to another type B1 CAI, Allende TS-34. This large (~1.2 cm) CAI contains numerous spinels that range up to ~150 μm in

size, ideal for performing detailed in situ chemical/isotopic studies on individual grains. The present work documents systematic relationships between minor element compositions of spinel inclusions in clinopyroxene or melilite and the local composition of the host phases for Allende TS-34, Allende TS-23, and Leoville 3537–2. We show that this object has also experienced at least one partial-melting event after its initial formation, but that subsolidus re-equilibration is also likely important. We exploit the large spinel grains present in TS-34 to compare oxygen isotopic compositions, as analyzed in situ, of spinels with their petrography and minor element concentrations. The oxygen data confirm that the thermal history of TS-34 resulted in significant subsolidus isotopic and chemical exchange.

EXPERIMENTAL TECHNIQUE

A total of 246 spinels and their host silicates in Allende TS-34 (known henceforth as TS-34) were analyzed following the procedures of Connolly and Burnett (1999). We designated individual spinel grains as edge, middle, or center according to their location within the inclusion and used high (400 nA) beam current for electron microprobe analyses of the spinels in order to obtain high precision minor element data (typically, 3% standard deviations at 0.1% concentration). Silicate compositions of host spinels were analyzed approximately 50μm from spinel grains, with one analysis per silicate referenced to each analyzed spinel grain for TS-34, Allende TS-23, and Leoville 3537–2. In addition to systematically documenting the relationships between the petrography and minor element chemistry of spinels and their host silicates, we also performed traverses across 6 spinel grains with 20 analyses per grain (crystal edge to edge). Similar analyses could not be performed on the inclusions investigated by Connolly and Burnett (1999) because of the small sizes of those grains. Following the procedure of Connolly and Burnett (1999), any spinel grain with 1000 ppm Si or greater was eliminated from our data because the analysis is suspect to contamination from enclosed silicates.

A total of 7 spinel grains and their host clinopyroxene and melilite grains were chosen for analysis of their oxygen isotopic compositions. Oxygen isotopic abundances were determined with the UCLA CAMECA ims 1270 ion microprobe utilizing techniques similar to those described previously (McKeegan et al. 1998; Simon et al. 2000). A Cs^+ primary ion beam was used to sputter shallow craters of ~20 μm diameter. Negative secondary ions were analyzed without energy filtering at high mass resolving power ($m/\Delta m$ >6500), sufficient to remove all molecular ion interferences. Charge compensation was achieved with the use of a normal-incidence electron gun (Slodzian, Chainteau, and Dennebouy 1987). Measurements were performed by magnetic peak switching and collecting the intense $^{16}O^-$ current (60–80 × 10^6 ions/sec equivalent) in a Faraday cup (FC) detector and the minor isotopes, $^{17}O^-$ and $^{18}O^-$, with an electron multiplier (EM). Measured ion ratios were corrected for background (FC), deadtime (EM), as well as instrumental mass fractionation (IMF) and relative detector efficiencies (EM/FC ratio) by comparison with analyses of a Burma spinel standard interspersed with those of the unknowns. The reported (1σ) uncertainties reflect both the internal measurement precision on an individual analysis and the reproducibility of repeated measurements of the spinel standard during the analysis session. Possible systematic errors in the IMF correction due to 'matrix effects' among the minerals considered here are negligible under our experimental conditions (Simon et al. 2000), and analyses are considered accurate at a level commensurate with the stated precision (typically ~1.5 to 2‰ in both $\delta^{17}O$ and $\delta^{18}O$).

RESULTS

Petrography

The relevant petrographic features of Leoville 3537–2 and Allende TS-23 are summarized in Connolly and Burnett (1999). Here, we focus on TS-34 (originally A13S4, Clayton et al. 1977), which is one of the largest known type B inclusions, measuring ~1.2 cm at its longest diameter (from the studied section), and has been extensively investigated (Clayton et al. 1977; Beckett 1986; Simon, Grossman, and Davis 1991; Davis, Simon, and Grossman 1992; Simon et al. 1996; Beckett, Simon, and Stolper 2000). Typical of B1 inclusions, TS-34 shows a well-defined mantle of melilite containing 4 vol% spinel and 38 vol% clinopyroxene, the latter occurring as small, anhedral inclusions within the melilite (Beckett 1986). The core contains ~14 vol% spinel, 32 vol% melilite, 46 vol% clinopyroxene, and <2 vol% anorthite, the remainder being alteration (Beckett 1986). Type B clinopyroxenes (referred to as fassaite in many CAI papers) contain exceptionally high concentrations of Al, Ti^{+3}, and Ti^{+4} (e.g., Simon, Grossman, and Davis 1991). A general trend exists within TS-34 in the distribution of spinel grain sizes, with the coarser spinels in the core grading to finer ones in the mantle melilite. Numerous cracks and veins of alteration, typical of Allende inclusions, are present throughout the inclusion.

Spinel Minor Element Chemistry: Comparison of TS-34 with Leoville 3537-2 and Allende TS-23

An overall positive correlation exists between the V and Ti concentrations of TS-34 spinels (Fig. 1, Table 1). However, the striking aspect of Fig. 1a is the compositional groupings according to location. The highest V concentrations (approaching 1 wt%) are found in edge spinels. Spinels from

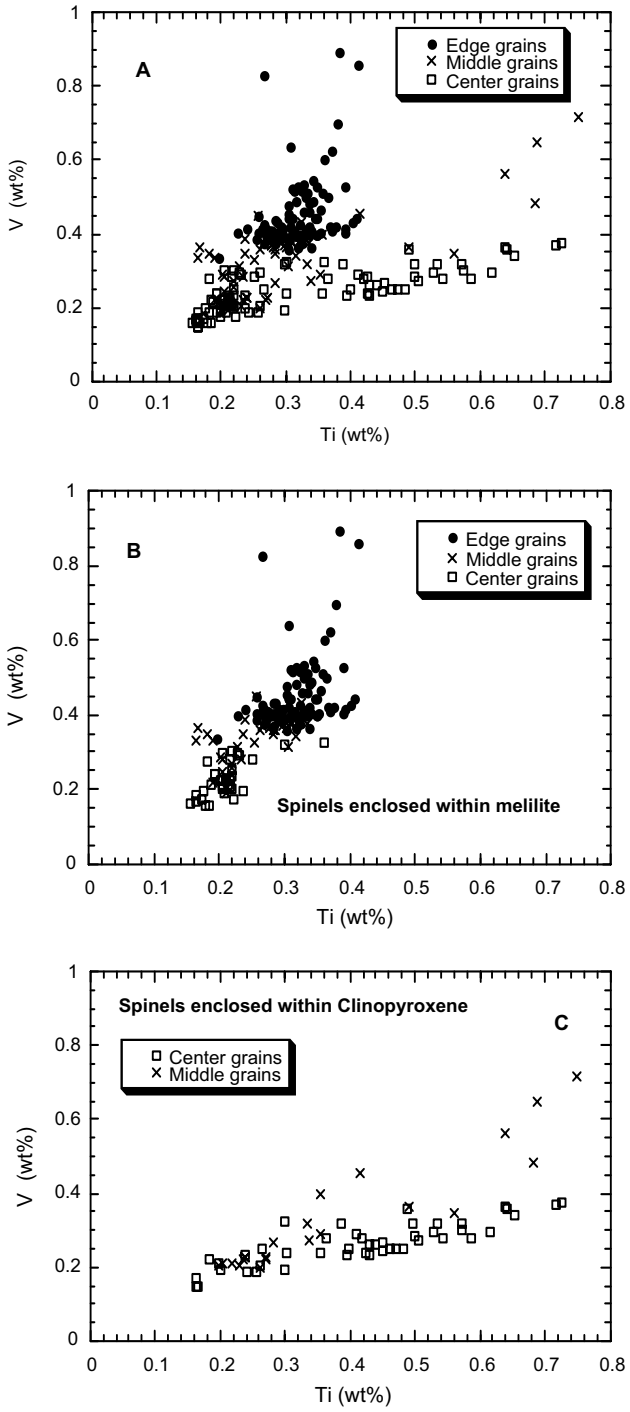

Fig. 1. a) Plot of V (wt%) versus Ti (wt%) for spinels from Allende TS-34. Closed symbols represent those grains that are from edge areas, Xs and open squares are from middle and center (core) areas of the inclusion. The overall range in V and Ti is much greater than that expected for a single-stage igneous history; b) The data from (a) with the analyses from spinel enclosed only by melilite plotted; c) The data from (a) with only the analyses from spinels enclosed by clinopyroxene shown. Error associated with each analysis is approximately the same size as the symbols. If errors bars are plotted, many of the differences between data points become obscured. Thus, we have not shown these.

the center of TS-34 are distinct, showing a smaller range of V (0.15–0.4 wt%) and a larger range (0.16–0.75 wt%) of Ti. The middle grains are compositionally intermediate.

Equally striking is that the spinel grains can be further grouped based on their host silicate phase (Figs. 1b and 1c). Spinels enclosed in melilite (Fig. 1b) show a positive trend that is separate from grains enclosed in clinopyroxene (Fig. 1c), with some overlap existing at the lowest V and Ti values. A gap in the Ti values between the two groups is present in the sense that no high-Ti spinels (>0.45 wt%) exist within melilite.

Fig. 1 represents our most important correlation. Except for overall higher V and Ti concentrations in TS-34 spinels, similar patterns were observed in both Leoville 3537–2 and Allende TS-23 (Connolly and Burnett 1999), suggesting that the trends shown in Fig. 1 are a general property of type B CAIs. The higher Ti in TS-34 spinels compared to those in Allende TS-23 reflects the higher bulk Ti concentration in TS-34 (Beckett 1986).

There is a wide range of Fe concentrations in spinel (0.02 to >1 wt%). In all inclusions studied there is no correlation of spinel Fe content with that of any other minor element. There are, however, intra- and inter-sample differences. Consequently, we use a compact, but appropriate, data representation based on one-dimensional histograms. In Fig. 2, each Fe analysis is plotted on the y axis with the different samples separated along the x axis using an arbitrary sample number. This representation suppresses quantitative frequency information compared to a two-dimensional histogram, although frequency information is qualitatively expressed by the density of points. The disadvantage of this type of histogram is outweighed by the convenience in inter-sample comparisons using Fig. 2. Most importantly, we have no useful interpretative framework for typical two-dimensional histograms. Quantitative data are available on request from the authors. For all inclusions, edge, center, and middle regions are indicated. For TS-34, where a large number of analyses are available, we separately plot different distinct locations within a given region. Although a very large range in Fe concentration is observed for Allende TS-23, the fraction of Fe-rich grains increases from center to middle to edge. This is understandable if the Fe in spinel is incorporated during secondary alteration processes. The TS-34 Fe distribution is qualitatively the same as that for Allende TS-23, although the fraction of grains with Fe >0.1 wt% is less for TS-34. This correlates with a greater amount of alteration phases in Allende TS-23 than in TS-34 (Beckett 1986). The Allende (TS-34 and TS-23) distributions are much broader and skewed to higher Fe concentrations than the relatively unaltered inclusion Leoville 3527–2 (Connolly and Burnett 1999) where only 1 of 117 grains has >0.1% Fe. In comparison with TS-23, where many spinels with Fe >1 wt% are observed, the alteration process in TS-34, although pervasive, was apparently not as effective, or the source of Fe

Table 1. Minor element concentrations of spinels from Allende TS-34. Analytical uncertainty associated with the data are approximately ±0.02 for Ca, Ti, V, and Cr; ±0.03 for Fe.[a]

Sample #	Host	Ca wt%	Ti wt%	V wt%	Cr wt%	Fe wt%
Edge 1						
sp1c	Mel	0.06	0.35	0.40	0.11	0.06
sp2	Mel	0.07	0.34	0.40	0.11	0.06
sp3	Mel	0.08	0.32	0.38	0.10	0.08
sp4	Mel	0.10	0.28	0.37	0.10	0.93
sp5	Mel	0.10	0.27	0.39	0.11	1.21
sp6	Mel	0.08	0.28	0.40	0.09	0.30
sp7	Mel	0.08	0.28	0.40	0.10	0.25
sp8	Mel	0.18	0.32	0.40	0.09	0.16
sp9	Mel	0.11	0.28	0.40	0.09	0.44
sp11	Mel	0.12	0.30	0.39	0.08	0.28
sp12	Mel	0.05	0.29	0.39	0.08	0.30
sp13	Mel	0.12	0.27	0.41	0.06	0.15
sp14	Mel	0.10	0.27	0.42	0.06	0.12
sp15	Mel	0.10	0.26	0.40	0.06	0.17
sp17	Mel	0.09	0.39	0.42	0.10	0.03
sp18c	Mel	0.05	0.39	0.40	0.10	0.03
sp19	Mel	0.06	0.37	0.41	0.09	0.03
sp20	Mel	0.10	0.35	0.41	0.09	0.04
sp21	Mel	0.07	0.33	0.40	0.09	0.04
sp22	Mel	0.08	0.33	0.40	0.09	0.04
sp23	Mel	0.06	0.35	0.40	0.09	0.03
sp24	Mel	0.12	0.34	0.41	0.09	0.08
sp25	Mel	0.11	0.38	0.42	0.09	0.03
sp26	Mel	0.09	0.26	0.45	0.08	0.66
sp27c	Mel	0.07	0.32	0.49	0.09	0.14
sp29	Mel	0.08	0.36	0.50	0.09	0.02
sp30	Mel	0.13	0.30	0.45	0.09	0.14
sp31	Mel	0.07	0.31	0.44	0.08	0.09
sp32	Mel	0.08	0.34	0.46	0.08	0.04
sp33	Mel	0.05	0.35	0.44	0.08	0.03
sp34	Mel	0.09	0.31	0.53	0.09	0.07
sp36c	Mel	0.08	0.28	0.44	0.08	0.13
sp37c	Mel	0.06	0.31	0.44	0.09	0.04
sp38	Mel	0.18	0.41	0.44	0.09	0.03
sp39	Mel	0.08	0.29	0.43	0.08	0.35
sp40	Mel	0.07	0.35	0.45	0.09	0.02
sp41	Mel	0.06	0.34	0.42	0.08	0.07
sp42	Mel	0.09	0.33	0.41	0.08	0.05
sp43	Mel	0.06	0.32	0.43	0.08	0.06
sp44	Mel	0.14	0.31	0.41	0.08	0.13
sp45	Mel	0.05	0.37	0.42	0.08	0.06
sp46	Mel	0.06	0.40	0.43	0.08	0.04
Edge 2						
sp1c	Mel	0.08	0.27	0.37	0.13	0.06
sp2c	Mel	0.08	0.27	0.41	0.13	0.04
sp3	Mel	0.11	0.27	0.41	0.14	0.06
sp4a	Mel	0.08	0.26	0.41	0.14	0.03
sp5a	Mel	0.08	0.23	0.40	0.14	0.15
sp6	Mel	0.13	0.24	0.42	0.14	0.25
sp7	Mel	0.06	0.27	0.43	0.14	0.12
sp8	Mel	0.06	0.29	0.42	0.14	0.08
sp9c, a	Mel	0.07	0.29	0.40	0.12	0.04
sp10	Mel	0.06	0.31	0.44	0.13	0.07
sp11	Mel/Cpx	0.06	0.30	0.42	0.11	0.08
sp12c	Mel/Cpx	0.16	0.31	0.42	0.11	0.04
sp13c	Mel/Cpx	0.10	0.28	0.41	0.11	0.09
sp14	Mel/Cpx	0.12	0.27	0.40	0.10	0.05
sp15	Mel	0.08	0.28	0.41	0.10	0.08
sp16	Mel/Cpx	0.08	0.29	0.40	0.10	0.05
sp17	Mel/Cpx	0.11	0.31	0.40	0.10	0.03
sp18c	Mel	0.06	0.31	0.39	0.09	0.08
sp19	Mel	0.08	0.34	0.40	0.10	0.03
sp20	Mel	0.11	0.31	0.40	0.09	0.04
sp21	Mel	0.15	0.26	0.39	0.08	0.03
sp22a	Mel	0.08	0.32	0.37	0.09	0.07
sp23a	Mel	0.11	0.20	0.34	0.09	0.50
sp24	Mel	0.09	0.34	0.36	0.08	0.02
sp25c	Mel	0.09	0.30	0.36	0.08	0.06
Edge 3						
sp1c	Mel	0.06	0.34	0.55	0.11	0.05
sp2	Mel	0.05	0.36	0.60	0.11	0.21
sp3	Mel	0.17	0.37	0.63	0.14	0.14
sp4	Mel	0.08	0.27	0.83	0.17	0.54
sp5c	Mel	0.09	0.38	0.70	0.14	0.06
sp6	Mel	0.07	0.39	0.53	0.11	0.06
sp7c	Mel	0.06	0.31	0.64	0.13	0.26
sp8c	Mel	0.05	0.33	0.51	0.11	0.19
sp9c	Mel	0.08	0.35	0.53	0.12	0.17
sp10	Mel	0.10	0.34	0.48	0.10	0.09
sp11	Mel	0.13	0.35	0.46	0.10	0.15
sp12c	Mel	0.09	0.32	0.52	0.11	0.33
sp13c	Mel	0.09	0.30	0.48	0.10	0.28
sp14c	Mel	0.10	0.33	0.46	0.10	0.23
sp15	Mel	0.07	0.33	0.51	0.11	0.13
sp16	Mel	0.14	0.33	0.53	0.12	0.28
sp16	Mel	0.08	0.31	0.52	0.11	0.11
sp17c	Mel	0.08	0.32	0.53	0.12	0.11
sp18	Mel	0.06	0.38	0.89	0.21	0.17
sp19c	Mel	0.13	0.41	0.86	0.20	0.05
sp20c	Mel	0.09	0.34	0.49	0.11	0.09
sp21c	Mel	0.07	0.36	0.51	0.12	0.11
sp22c	Mel	0.12	0.33	0.50	0.11	0.19
Middle 1						
Sp1c	Mel	0.03	0.32	0.38	0.12	0.05
Sp2c	Mel	0.05	0.31	0.39	0.13	0.04
Sp3	Mel	0.06	0.33	0.39	0.13	0.03
Sp4c	Mel	0.05	0.28	0.40	0.12	0.08
Sp5	Mel	0.07	0.27	0.37	0.13	0.05
Sp6c	Mel	0.07	0.29	0.38	0.13	0.04
Sp7a	Mel	0.06	0.30	0.38	0.13	0.03
Sp8a	Mel	0.09	0.26	0.36	0.13	0.03
Sp9	Mel	0.06	0.31	0.38	0.12	0.03
Sp10c	Mel	0.04	0.28	0.37	0.12	0.09
Sp11	Mel	0.06	0.29	0.37	0.12	0.03
Sp12	Mel	0.09	0.32	0.38	0.12	0.03
Sp13a	Mel	0.04	0.25	0.33	0.12	0.09
Sp14a	Mel	0.10	0.32	0.34	0.12	0.03
Sp15	Mel	0.09	0.34	0.38	0.12	0.03
Sp16	Mel	0.07	0.30	0.37	0.11	0.03
Sp17	Mel	0.09	0.31	0.38	0.11	0.03
Sp18a	Mel	0.05	0.32	0.39	0.11	0.03
Sp19c	Mel	0.06	0.31	0.39	0.11	0.03
Sp20a	Mel	0.06	0.31	0.40	0.11	0.04
Sp21a	Mel	0.06	0.28	0.37	0.11	0.15
Sp22	Mel	0.08	0.28	0.36	0.10	0.03
Sp23	Mel	0.12	0.30	0.36	0.13	0.05
Sp24a	Mel	0.05	0.24	0.35	0.11	0.10
Sp25	Mel	0.08	0.28	0.36	0.11	0.09
Sp26	Mel	0.08	0.28	0.38	0.11	0.09
Middle 2						
sp1c	Mel	0.05	0.20	0.29	0.10	0.17

Table 1. Minor element concentrations of spinels from Allende TS-34. Analytical uncertainty associated with the data are approximately ±0.02 for Ca, Ti, V, and Cr; ±0.03 for Fe.[a] *Continued.*

Sample #	Host	Ca wt%	Ti wt%	V wt%	Cr wt%	Fe wt%
sp2c	Mel	0.08	0.19	0.33	0.10	0.05
sp3c	Mel/Cpx	0.05	0.17	0.33	0.09	0.11
sp4c	Mel	0.10	0.18	0.35	0.09	0.09
sp5c	Mel/Cpx	0.04	0.26	0.45	0.11	0.15
sp6	Mel	0.15	0.17	0.36	0.10	0.11
sp7	Mel/Cpx	0.02	0.31	0.32	0.08	0.08
sp8c	Mel/Cpx	0.02	0.28	0.35	0.09	0.05
sp9c	Mel	0.03	0.24	0.39	0.09	0.04
sp10c	Mel/Cpx	0.02	0.27	0.40	0.09	0.04
sp11c	Mel/Cpx	0.03	0.33	0.43	0.09	0.05
sp12	Mel/Cpx	0.08	0.21	0.28	0.09	0.06
sp13	Mel	0.08	0.23	0.31	0.09	0.03
sp14	Mel	0.03	0.23	0.28	0.08	0.03
sp15c	Mel	0.05	0.22	0.27	0.09	0.02
sp16	Mel	0.07	0.22	0.26	0.10	0.07
sp17c	Mel/Cpx	0.02	0.19	0.22	0.09	0.07
sp18	Mel	0.03	0.20	0.25	0.10	0.04
sp19c	Cpx	0.08	0.49	0.36	0.09	0.35
sp20c	Cpx	0.05	0.56	0.35	0.09	0.10
sp21c	Cpx	0.06	0.42	0.45	0.09	0.45
sp22c	Cpx	0.05	0.28	0.27	0.09	0.05
sp23c	Cpx	0.04	0.20	0.21	0.09	0.19
sp24c	Cpx/Mel	0.04	0.33	0.32	0.09	0.06
sp25	Cpx	0.06	0.34	0.27	0.09	0.09
sp26	Cpx	0.08	0.24	0.23	0.09	0.15
sp27	Cpx/Mel	0.03	0.24	0.22	0.10	0.05
sp28	Cpx	0.02	0.24	0.23	0.09	0.04
sp29	Cpx	0.03	0.35	0.29	0.09	0.06
sp30c	Cpx	0.02	0.27	0.23	0.10	0.06
sp31	Cpx	0.02	0.22	0.21	0.10	0.07
sp32	Cpx/Mel	0.03	0.20	0.20	0.10	0.09
sp33	Mel	0.04	0.21	0.20	0.10	0.06
sp34	Mel	0.06	0.21	0.19	0.10	0.04
sp35	Cpx	0.03	0.26	0.20	0.10	0.10
sp36	Cpx	0.02	0.27	0.22	0.10	0.10
sp38	Cpx/Mel	0.02	0.23	0.20	0.10	0.06
sp39	Cpx/Mel	0.03	0.69	0.65	0.17	0.09
sp40	Cpx	0.04	0.68	0.49	0.09	0.05
sp41	Cpx	0.03	0.75	0.71	0.16	0.29
sp42	Cpx	0.02	0.36	0.40	0.11	0.06
sp43	Cpx	0.07	0.64	0.56	0.18	0.42
Center 1						
sp1	Cpx	0.02	0.47	0.25	0.14	0.03
sp2	Cpx	0.02	0.39	0.23	0.15	0.06
sp3	Cpx	0.02	0.53	0.30	0.14	0.03
sp4	Cpx	0.02	0.46	0.25	0.15	0.05
sp5c	Cpx	0.02	0.43	0.24	0.14	0.06
sp6	Cpx	0.03	0.44	0.26	0.14	0.06
sp7	Cpx	0.03	0.45	0.27	0.14	0.04
sp8c	Cpx	0.03	0.62	0.30	0.13	0.07
sp9c	Cpx	0.03	0.57	0.30	0.12	0.05
sp10c	Cpx	0.02	0.41	0.29	0.12	0.04
sp11c	Cpx	0.05	0.26	0.20	0.13	0.12
sp12	Cpx	0.06	0.65	0.34	0.11	0.04
sp13c	Mel/Cpx	0.04	0.26	0.30	0.11	0.03
sp14	Cpx	0.03	0.64	0.36	0.10	0.03
sp15	Cpx	0.04	0.64	0.36	0.09	0.02
sp16	Mel/Cpx	0.06	0.18	0.28	0.11	0.08
sp17	Mel/Cpx	0.04	0.25	0.28	0.11	0.08
sp18	Mel	0.02	0.43	0.29	0.10	0.05
sp19	Mel/Cpx	0.02	0.30	0.32	0.10	0.02
sp20	Mel/Cpx	0.05	0.36	0.32	0.10	0.02
sp22	Mel	0.03	0.21	0.23	0.11	0.03
sp23	Mel	0.09	0.22	0.25	0.11	0.03
sp24	Mel	0.04	0.22	0.20	0.10	0.03
sp25	Mel	0.04	0.21	0.20	0.11	0.03
sp26	Mel	0.05	0.21	0.21	0.10	0.05
sp27	Mel	0.07	0.22	0.21	0.10	0.04
sp28	Mel	0.06	0.18	0.16	0.10	0.03
sp29	Mel/An	0.04	0.18	0.16	0.09	0.03
sp30	Mel/Cpx	0.05	0.19	0.24	0.09	0.07
sp31	Mel	0.07	0.22	0.30	0.08	0.03
sp32	Mel	0.05	0.23	0.29	0.09	0.03
sp33	Mel	0.06	0.21	0.30	0.08	0.05
sp34c	Cpx	0.03	0.73	0.38	0.08	0.04
sp35	Cpx	0.06	0.72	0.37	0.07	0.03
Center 2						
sp1c	Mel	0.04	0.21	0.21	0.09	0.03
sp2c	Mel/Cpx	0.03	0.16	0.18	0.10	0.11
sp3c	Mel/Cpx	0.02	0.22	0.17	0.10	0.03
sp4c	Cpx	0.02	0.43	0.23	0.09	0.03
sp5	Cpx	0.02	0.45	0.25	0.09	0.03
sp6	Cpx	0.02	0.39	0.32	0.09	0.02
sp7	Cpx	0.08	0.19	0.22	0.10	0.03
sp8c	Cpx/Mel	0.09	0.20	0.21	0.09	0.12
sp9c	Mel/Cpx	0.03	0.24	0.20	0.09	0.09
sp10	Mel	0.07	0.23	0.30	0.08	0.04
sp11c	Mel	0.09	0.22	0.28	0.09	0.03
sp12	Mel	0.07	0.16	0.16	0.09	1.40
sp13c	Mel	0.05	0.21	0.23	0.09	0.18
sp14c	Mel	0.03	0.20	0.22	0.09	0.04
sp15	Cpx	0.03	0.36	0.28	0.09	0.05
sp16	Cpx	0.06	0.42	0.28	0.09	0.12
sp17c	Cpx	0.03	0.53	0.32	0.09	0.10
sp18	Cpx	0.05	0.50	0.32	0.09	0.11
sp19c	Cpx	0.02	0.27	0.25	0.09	0.10
sp20	Cpx	0.05	0.57	0.32	0.09	0.05
sp21	Cpx	0.02	0.51	0.27	0.09	0.03
sp22c	Cpx	0.02	0.43	0.26	0.09	0.10
sp23	Cpx	0.03	0.36	0.24	0.09	0.07
sp24	Cpx	0.02	0.24	0.19	0.10	0.04
sp25	Mel/Cpx	0.03	0.20	0.18	0.10	0.03
sp26c	Cpx/Mel	0.04	0.16	0.15	0.12	0.06
sp27	Cpx/Mel	0.05	0.20	0.19	0.11	0.15
sp28c	Cpx	0.05	0.17	0.15	0.11	0.13
sp29	Mel	0.03	0.17	0.17	0.10	0.04
sp30	Mel	0.05	0.16	0.17	0.11	0.03
Center 3						
sp1c	Cpx	0.02	0.50	0.29	0.09	0.04
sp2	Cpx	0.02	0.54	0.28	0.10	0.04
sp3	Cpx	0.02	0.48	0.25	0.09	0.03
sp4	Cpx	0.02	0.59	0.28	0.09	0.03
sp5	Cpx	0.02	0.49	0.36	0.12	0.10
sp6	Cpx	0.03	0.30	0.24	0.09	0.04
sp7	Cpx	0.03	0.40	0.25	0.11	0.49
sp8c	Cpx	0.02	0.26	0.19	0.10	0.05
sp9	Cpx	0.03	0.30	0.20	0.09	0.03
sp10	Mel/Cpx	0.03	0.22	0.20	0.10	0.06
sp11	Mel	0.05	0.18	0.19	0.10	0.25
sp12	Mel	0.05	0.19	0.19	0.10	0.03
sp13c	Cpx/Mel	0.07	0.17	0.16	0.10	0.11
sp20	Mel/Cpx	0.05	0.36	0.32	0.10	0.02

Table 1. Minor element concentrations of spinels from Allende TS-34. Analytical uncertainty associated with the data are approximately ±0.02 for Ca, Ti, V, and Cr; ±0.03 for Fe.[a] *Continued.*

Sample #	Host	Ca wt%	Ti wt%	V wt%	Cr wt%	Fe wt%	Sample #	Host	Ca wt%	Ti wt%	V wt%	Cr wt%	Fe wt%
sp14	Cpx/Mel	0.03	0.16	0.17	0.10	0.05	sp20	Cpx	0.04	0.24	0.23	0.10	0.07
sp15	Mel	0.03	0.21	0.19	0.10	0.03	sp21	Mel	0.03	0.19	0.21	0.10	0.03
sp16	Mel	0.02	0.20	0.22	0.10	0.04	sp22	Mel	0.05	0.17	0.20	0.10	0.02
sp17	Mel	0.05	0.19	0.24	0.10	0.24	sp23	Cpx/Mel	0.04	0.30	0.32	0.09	0.05
sp18	Mel/Cpx	0.03	0.22	0.24	0.10	0.08	sp25	Cpx	0.04	0.16	0.17	0.10	0.24
sp19	Mel/Cpx	0.02	0.22	0.22	0.10	0.09							

[a]Sp = spinel; Host = silicate phase that spinel is enclosed within; Mel = melilite; Cpx = clinopyroxene (often referred to by the unofficial name of fassaite). If both phases are indicated, then a grain is between both melilite and clinopyroxene; c indicates that the designated spinel grain contains a crack of unknown origin that often propagates into the surrounding host silicate phase; a indicates that the designated spinel grain is located within an area of melilite alteration that was determined qualitatively by texture and EDS measurements.

not sufficient, to produce Fe enrichments similar to those observed in TS-23.

Most TS-34 spinels have Cr concentrations in the restricted range of 0.075–0.15 wt% (Fig. 3). There is no correlation with other minor elements except for the Edge 3 subpopulation (Fig. 3b) that shows a distinct positive V-Cr correlation that is not found in the other edge locations. The previously studied inclusions have essentially the same range in spinel Cr. The Edge 3 correlation has no analog in the previously studied inclusions (Connolly and Burnett 1999), although the Leoville inclusion shows a distinct inverse overall Cr-V correlation. Many of the high V edge grains in Allende TS-23 show high Fe and low Cr concentrations, but this sub-population was not found in TS-34.

There is no correlation of spinel Ca concentration with any other minor element. Consequently, the same representation is used for Ca in Fig. 4 as was used for Fe in Fig. 2. Overall, there is no correlation of Ca concentration with grain size, somewhat allaying concerns about continuum secondary fluorescence effects in the Ca analyses. However, Ca profiles in the largest individual TS-34 spinels are always edge enriched which could be an artifact due to continuum secondary fluorescence, at least in the outer 10 microns. The Ca concentrations in the cores of these large grains are 0.02–0.04%, consistent with, but not lower than, the general range of individual TS-34 center grain Ca analyses from Fig. 4. One large spinel grain (sp10) straddled a boundary between melilite and clinopyroxene, but the Ca profile across the spinel grain was symmetric despite the fact that the Ca concentration of melilite is 60% higher than the clinopyroxene. Because the Ca analyses were typically done on grains 20 microns and larger, we consider that they are not seriously affected by continuum secondary fluorescence, but more work would be required to establish this conclusively. In TS-34, the grains from all 3 edge locations tend to have systematically higher Ca than the grains from 3 center locations, but this difference is not seen in TS-23 or in Leoville 3537–2. This is in the right direction to be explained by continuum secondary fluorescence because the large spinel grains are in the center regions of TS-34. However, continuum secondary fluorescence effects of the order of 1000 ppm are required and this, we think, is excessively large.

Variations Within Individual TS-34 Spinel Grains

The large spinel grains in TS-34 provide a unique opportunity to explore minor element zoning relationships. We measured 11 orthogonal profiles on 6 large (about 80 micron) grains, including both spinel inclusions in melilite and in clinopyroxene. All grains were in the center part of the inclusion.

Fe is usually enriched in the rims, presumably reflecting post-solidification alteration. The core Fe values are around 0.03 wt%, consistent with the minimum values for small grains on Fig 2.

Zoning profiles can be difficult to interpret because, unless the plane of the section goes through the core, the true extent of zoning is suppressed. Even allowing for this, the zoning patterns for Ti, V, and to a lesser extent Cr, are complex and not easily interpreted. No single grain is homogeneous in Ti and V at the two standard deviation level, although 2/22 individual profiles are uniform at this level (4–5%). Although absolute variations are not large (<50%) and are much less than the intergrain variations discussed above, they are far in excess of analytical errors. Cr variations tend to be smaller with 4/11 profiles homogeneous at 2 standard deviations (about 5%). Clear cases of simple core-rim variations for these elements are overall absent. Some profiles show chaotic variations, which in the terminology of Beckett et al. (2000) would be referred to as "non-distal" zoning. Some Ti and V profiles are monotonic, increasing from one end of the grain to the other. Complete data files are available from the authors on request.

In principle, the trends in Ti and V in spinel grains hosted by clinopyroxene (Figs. 8 and 9) could be affected by continuum secondary fluorescence. However, we do not believe this to be significant for 3 reasons: 1) Although the Ti concentration of the clinopyroxene is high, that of the spinel is also relatively high (0.2–0.7%), thus the "chemical contrast" between the spinel and surrounding clinopyroxene is not especially large (Ti_{cpx}/Ti_{sp} = 13). A large chemical contrast is required for continuum secondary fluorescence to be important. For comparison, the equivalent chemical contrast for Ca between spinel and melilite, where we are concerned about continuum secondary flourescence, is 570.

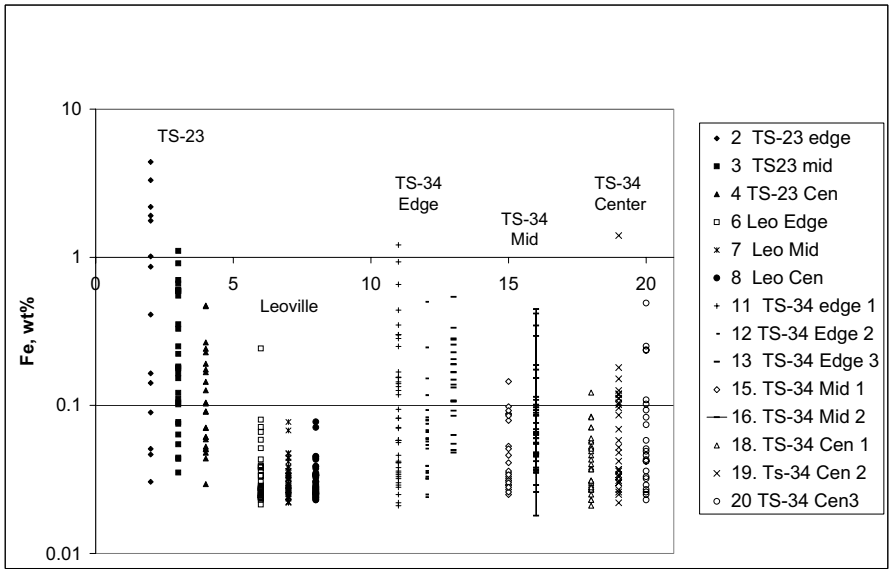

Fig. 2. One-dimensional histograms of Fe (wt%) in spinels from the three inclusions studied. In all cases, the edge, middle, and center locations are plotted separately. For TS-34, for which there are a large number of analyses, the data for different locations in a given region are plotted separately. The x axis is a sample number, identified in the legend. There is a large range of Fe concentrations, but there is no correlation of Fe with V (or any other major element). The substantially lower Fe concentrations in Leoville almost certainly reflect the overall lack of alteration in this inclusion. The overall levels of Fe in TS-34 tend to be intermediate relative to those from Allende TS-23 and Leoville 3537–2, correlating with the intermediate degree of alteration for TS-34

For V between spinel and clinopyroxene, the chemical contrast is ≈1, so it is clear that continuum secondary fluorescence is negligible in this case. 2) In many cases, especially in TS-34, the V and Ti spinel analyses were made in the centers of grains of 100 μm size at distances from the clinopyroxene boundary where the effects of continuum secondary fluorescence are small. Moreover, large grains do not show the lowest Ti and V concentrations. 3) Finally, if continuum secondary fluorescence was important, steep gradients of Ti from edge to center in the larger spinel grains should always be present, but this is not observed. Thus, we conclude that continuum secondary fluorescence produces negligible effects on the Ti or V concentrations of spinel inclusions in clinopyroxene.

Relationships Between Compositions of Spinel Grains and Their Host Silicates

The relationships between V and Ti for spinel inclusions in melilite and the åkermenite content ($X_{Åk}$) of the surrounding melilite are shown in Figs. 5–7d (data for TS-34 are presented in Table 2) for all three inclusions studied. The data from all three CAIs are consistent with a bimodal distribution of $X_{Åk}$ around a value of 0.40 to 0.45, best documented for TS-34 for which a large number of analyses are available. The spinel V and Ti concentrations are significantly lower in high Åk melilite, as would be anticipated from Fig. 1 and the well-established rim to center increases in Åk content for type B CAIs.

For grains with $X_{Åk}$ >0.4, there is an apparent overall trend of decreasing V with increasing $X_{Åk}$, particularly suggestive since it is seen in all three inclusions. However, there is also considerable scatter, especially in the TS-34 data. The Ti data for $X_{Åk}$ >0.4 are consistent with a similar trend to that for V, although there is more scatter, and the trend may be absent for TS-34. Especially for TS-34, the middle grains are a transitional population in that most, but not all, have adjacent melilite with Åk >0.45, but about half have Ti contents like those of the edge grains.

For TS-34 and Leoville 3537–2, a positive correlation exists between the Ti and V concentration of spinel inclusions in clinopyroxene and that of the surrounding clinopyroxene, although with considerable scatter in the TS-34 data (Figs. 8 and 9). Meeker, Wasserburg, and Armstrong (1983) noted similar trends in Ti between clinopyroxene and spinels. Especially striking are 4–6 middle spinel grains in TS-34 that show large variations in V with no variation in the adjacent clinopyroxene V. These same grains stand out as deviations from the V-Ti correlation in Fig. 1c. Part of the scatter in the TS-34 data undoubtedly results from the complex Ti and V clinopyroxene zoning patterns that complicates the assumption of a well-defined surrounding clinopyroxene composition. The clinopyroxene zoning patterns are simpler in Leoville 3537–2 and the correlations are better.

No correlation between any minor element content of spinels and their grain size was observed. We note that our data for silicates is only representative of potential relationships with compositions of the included spinels in that we did not map the silicate compositions in detail around each spinel grain. Such an approach might yield slight variations in

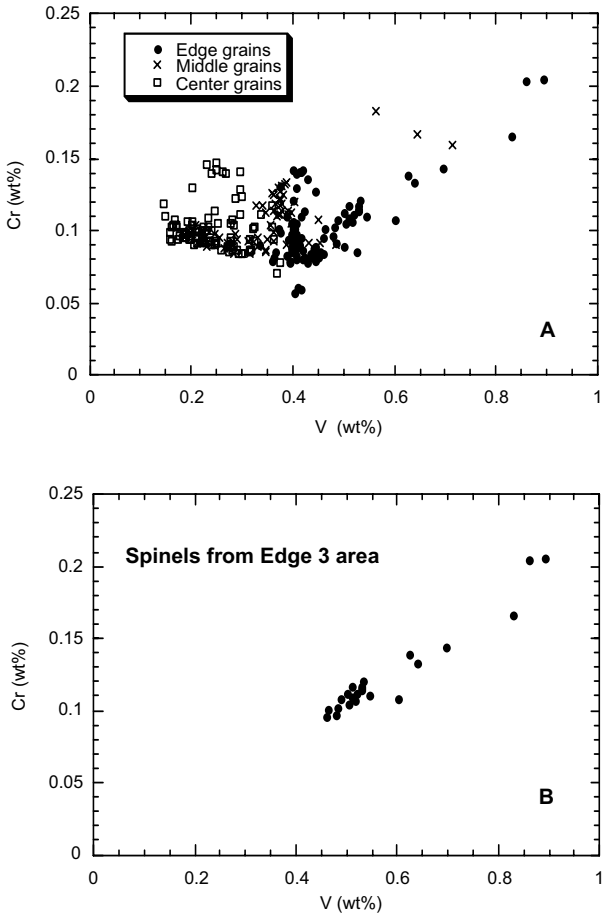

Fig.3. Plot of Cr (wt%) versus V (wt%) of spinels from TS-34. All data are shown in (a). Almost no correlation exist, except for edge area 3, where a positive relationship is observed, as shown explicitly in (b). Error associated with each analysis is approximately the same size as the symbols. If errors bars are plotted many of the differences between data points become obscured, thus we have not shown these.

the correlation trends compared to those reported here because the silicates are chemically zoned. We discuss this issue in slightly more detail below.

Oxygen Isotope Data

All TS-34 spinels analyzed (Table 3) are highly enriched in ^{16}O, with $\delta^{18}O$ values ranging from –48.1 ± 1.8‰ to –52.0 ± 1.6‰ (all errors are 1σ) and $\delta^{17}O$ values ranging from –49.3 ± 1.7‰ to –54.0 ± 1.6‰. The host clinopyroxene is less ^{16}O-rich with a $\delta^{18}O$ value of –40.8 ± 1.6‰ and a $\delta^{17}O$ value of –44.2 ± 1.8‰ (Table 4). The two melilites analyzed (Table 4) have $\delta^{18}O$ values from –0.9 ± 1.5‰ to –1.9 ± 1.6‰ and $\delta^{17}O$ values that range from –3.0 ± 1.2‰ to –3.5 ± 1.1‰. All data fall within error of the Allende CAI mixing line (Fig. 10a) and mineral compositions are generally consistent with those typically characteristic of type B CAIs (Clayton 1993; McKeegan and Leshin 2001), in the sense that spinel is the most ^{16}O-rich mineral, followed closely by pyroxene, with melilite much closer to the terrestrial mass fractionation line. Also shown (Figs. 10a and 10b) are mineral separate analyses made previously on a split of TS-34 (formerly called Al3S4) by Clayton and colleagues (Clayton et al. 1977). The agreement between the in situ and mineral separate analyses is good, with the exception of spinel (Fig. 10b) where the ion probe data show significantly (~10‰) higher ^{16}O-enrichments than the data for spinel separated from either pyroxene or melilite.

Four large spinel grains were analyzed from the central region and three from an edge region of the CAI. The center grains appear marginally more ^{16}O-enriched than the edge grains (mean $\Delta^{17}O$ = –25.5‰ compared to –24.8‰). However, this is not statistically significant and, in fact, all spinel grains analyzed are consistent with a single population (χ^2 = 0.6) with mean $\Delta^{17}O$ = –25.2 ± 0.5‰. Because the oxygen isotopic compositions of the various individual spinel grains are essentially the same, no correlation of $\Delta^{17}O$ exists either with minor element content, host silicate phase, or the proximity of the spinel to alteration veins or secondary silicates (Table 3).

DISCUSSION

Here we re-evaluate the conclusion of Connolly and Burnett (1999) that the minor element concentrations in CAI type B spinels indicate the re-melting of these objects following initial crystallization. We assume that, of the elements studied, Fe has definitely been affected by post-crystallization alteration and Cr may have been. Neither Cr nor Ca show any systematics to interpret. Moreover, there are still lingering doubts about continuum secondary fluorescence effects in the Ca data. Consequently, we focus our interpretations almost entirely on Ti and V.

Many alternatives to re-melting for producing the observed (Ti, V) compositional variations were considered by Connolly and Burnett (1999). With one exception, the problems with these alternatives remain, and are in fact enhanced, with the additional data reported here and will not be discussed further. The only viable alternative hypothesis to re-melting is local subsolidus re-equilibration of these elements, which we consider in detail below.

It is important to emphasize that, at present, the issue is not whether some type B1 CAIs have been remelted. This can be regarded as established independent of our work (e.g., Davis and MacPherson 1996; MacPherson and Davis 1993; Beckett, Simon, and Stolper 2000; Yangting and Kimura 2000). The focus here is whether the observed (Ti, V) systematics can be explained by re-melting or whether other processes must be invoked.

We begin by interpreting the (Ti, V) systematics for the two alternative hypotheses, then return to comparative

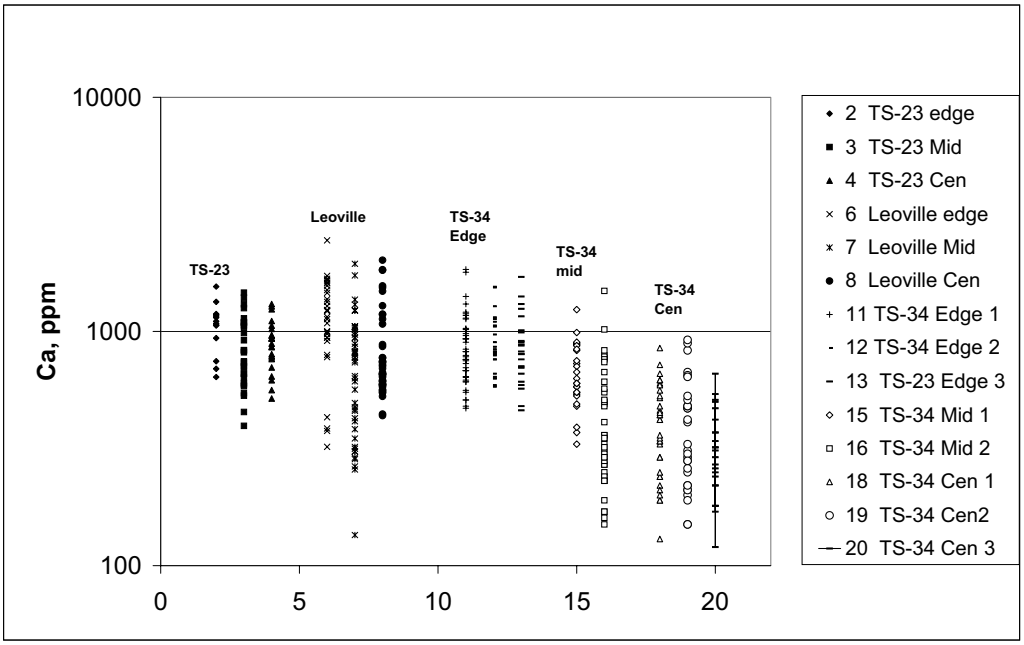

Fig. 4. One-dimensional histograms of Ca (wt%) in spinels from the three inclusions studied. In all cases, the edge, middle, and center locations are plotted separately. For TS-34, for which there are a large number of analyses, the data for different locations in a given region are plotted separately. The x axis is a sample number, identified in the legend. There are no correlations of Ca with other minor elements. TS-34 and Leoville 3537–2 show systematically higher Ca in edge spinels, but this is not seen in Allende TS-23. Allowance has not been made for the effects of continuum secondary fluorescence on the Ca analyses.

discussions of the sources of scatter as well as the zoning data and oxygen isotope compositions.

The Multiple-Melting of Type B CAIs

An important finding is that spinels enclosed within melilites form a trend in V and Ti that is different from that formed by spinels within clinopyroxenes (e.g., Fig. 1 and Connolly and Burnett 1999). The overall ranges of spinel V and Ti concentrations are much greater (almost an order of magnitude for V and a factor of 8 for Ti) than is expected for a single-stage crystallization history (Connolly and Burnett 1999). Significant constraints are added to a re-melting model if we include a discussion of the relationship between spinels and host silicates; this is a point that was not emphasized by Connolly and Burnett (1999).

Crystallization Sequence After Re-Melting

As justified below, the model is that a re-melting event partially reversed the initial crystallization sequence, melting all of the clinopyroxene and anorthite and part of the melilite and spinel. The great majority of spinels in the middle and center regions crystallized from the new liquid over a wide range of crystallization with large changes in liquid composition producing the corresponding large variations in spinel composition.

The absence of spinels with high Ti (>0.4 wt%) enclosed in melilite (Fig. 1) is striking and can be explained by the re-melting model. The same gap is present in Leoville 3537–2 and probably in TS-23 (Connolly and Burnett 1999), but the TS-34 data are particularly important in that it is unlikely that, out of our database of 246 analyzed spinels, we simply did not sample Ti-rich spinels in melilite.

In the context of the re-melting hypothesis, the lack of Ti-rich spinels in melilite requires that melilite must crystallize after clinopyroxene in the second-stage liquid. If melilite did not crystallize after clinopyroxene, we would expect to find spinels with higher Ti enclosed in melilites, and we do not. Thus, the fractional crystallization sequence of the new liquid generated from partial melting is required to be sp + clinopyroxene → melilite → anorthite.

The required crystallization sequence is consistent with known CAI phase equilibria. If, after its initial formation, TS-34 was reheated to temperatures (~1250–1350°C), below the spinel + liquid field, then only a fraction of the object would have remelted. Note that the transfer of thermal energy from the outside of the object to the core does not require that the outer mantle melilite melt. With respect to the phase diagram for type B CAIs defined by Stolper (1982), the bulk composition of the remelted portion of TS-34 would lie in the spinel + clinopyroxene field. Upon heating, all the anorthite and clinopyroxene dissolves, plus some melilite and spinel. Following the procedure of Beckett, Simon, and Stolper (2000) and guided by the change in V concentrations with host melilite $X_{Åk}$, we estimate that the temperature needed to melt melilite with $X_{Åk}$ >0.45 is approximately 1290°C. As it

Table 2. Election microprobe analyses (reported as wt%) of host silicate compositions for spinels listed in Table 1. Errors associated with analyses are approximately 0.02 for Na_2O, MgO, Ti_2O, FeO; 0.08 for Al_2O_3 and CaO; 0.05 for SiO_2; and 0.04 for V_2O_3.[a]

Sample #	Phase	Na_2O	MgO	Al_2O_3	SiO_2	CaO	TiO_2	FeO	V_2O_3	Totals
Edge 1										
sp1	Mel	bd	3.01	28.68	26.58	41.70	bd	bd	bd	99.97
sp2	Mel	bd	3.51	27.47	27.40	41.91	bd	bd	bd	100.29
sp3, 4, 5	Mel	bd	3.52	27.56	27.60	41.68	bd	bd	bd	100.36
sp6,7	Mel	bd	2.86	29.11	26.46	41.83	bd	bd	bd	100.26
sp8,9	Mel	bd	3.09	28.72	26.75	41.73	bd	bd	bd	100.29
sp10	Mel	bd	3.28	28.17	27.09	41.84	bd	bd	bd	100.38
sp11	Mel	bd	2.26	30.77	25.31	41.74	bd	bd	bd	100.08
sp12	Mel	bd	2.67	29.95	26.15	41.46	bd	bd	bd	100.23
sp13	Mel	bd	2.30	30.81	25.29	41.89	bd	bd	bd	100.29
sp14, 15	Mel	bd	3.68	32.37	24.94	38.62	bd	bd	bd	99.61
sp17	Mel	bd	3.58	27.49	27.31	41.69	bd	bd	bd	100.07
sp18	Mel	bd	3.57	27.25	27.25	41.81	bd	bd	bd	99.88
sp19, 20	Mel	bd	3.57	27.60	27.35	41.71	bd	bd	bd	100.23
sp21	Mel	bd	3.99	26.08	28.32	41.66	bd	bd	bd	100.05
sp22	Mel	bd	3.95	26.38	28.17	41.53	bd	bd	bd	100.03
sp23, 24	Mel	bd	3.90	25.85	27.90	41.32	bd	bd	bd	98.97
sp25	Mel	bd	4.02	25.29	28.25	41.78	bd	bd	bd	99.34
sp26, 27	Mel	bd	4.33	24.67	28.72	41.53	bd	bd	bd	99.25
sp28	Mel	bd	4.62	23.75	29.20	41.86	bd	bd	bd	99.43
sp29, 30	Mel	bd	3.96	25.36	27.89	41.79	bd	bd	bd	99.00
sp31	Mel	bd	4.16	25.23	28.52	41.82	bd	bd	bd	99.73
sp32	Mel	bd	4.54	24.00	29.02	41.89	bd	bd	bd	99.45
sp34	Mel	bd	5.06	22.80	29.77	41.40	bd	bd	bd	99.03
sp35	Mel	bd	4.83	23.90	29.46	41.67	bd	bd	bd	99.86
sp37	Mel	bd	4.65	24.46	29.35	41.85	bd	bd	bd	100.31
sp38	Mel	bd	3.88	26.65	28.08	41.99	bd	bd	bd	100.60
sp39	Mel	bd	4.72	24.25	29.67	41.96	bd	bd	bd	100.60
sp40	Mel	bd	3.88	26.52	28.03	41.90	bd	bd	bd	100.33
sp42	Mel	bd	3.81	26.78	27.91	41.78	bd	bd	bd	100.28
sp43	Mel	bd	4.56	24.76	29.13	41.97	bd	bd	bd	100.42
sp44	Mel	bd	3.94	26.34	28.20	41.78	bd	bd	bd	100.26
sp45, 46	Mel	bd	3.96	26.22	28.27	42.05	bd	bd	bd	100.50
Edge 2										
sp1	Mel	bd	4.64	25.08	29.16	41.73	bd	bd	bd	100.61
sp2	Mel	0.05	4.31	25.92	28.45	41.67	bd	bd	bd	100.40
sp3	Mel	bd	4.50	25.50	28.66	41.69	bd	bd	bd	100.35
sp4	Mel	bd	4.73	24.88	29.08	41.60	bd	bd	bd	100.29
sp5	Mel	0.03	4.98	24.29	29.42	41.87	bd	bd	bd	100.59
sp6	Mel	bd	4.91	24.35	29.50	41.56	bd	bd	bd	100.32
sp7, 8	Mel	0.10	5.51	23.40	30.78	40.01	bd	0.58	bd	100.38
sp9	Mel	bd	4.58	25.14	29.02	41.63	bd	bd	bd	100.37
sp10	Mel	bd	4.75	24.65	29.43	41.58	bd	bd	bd	100.41
sp11	Mel	0.04	5.01	23.72	29.85	41.26	bd	bd	bd	99.88
sp12, 13	Mel	0.06	4.83	24.30	29.48	41.59	bd	bd	bd	100.26
sp12, 13	Cpx	bd	8.70	20.66	37.37	25.30	8.28	bd	0.34	100.65
sp14	Mel	0.08	4.71	24.66	29.29	41.41	bd	bd	bd	100.15
sp15	Mel	0.01	5.03	24.03	29.77	41.84	bd	bd	bd	100.68
sp16	Mel	0.09	5.06	23.84	29.84	41.57	0.05	bd	bd	100.40
sp16	Cpx	NA	8.92	19.19	37.85	25.34	8.54	bd	0.44	100.28
sp17	Mel	bd	5.05	23.84	29.71	41.58	bd	bd	bd	100.18
sp18	Mel	0.04	5.44	22.76	30.64	41.56	bd	bd	bd	100.44
sp19	Mel	bd	4.80	24.25	29.44	41.61	bd	bd	bd	100.10
sp20	Mel	bd	4.91	24.26	29.74	41.44	bd	bd	bd	100.35

Table 2. Election microprobe analyses (reported as wt%) of host silicate compositions for spinels listed in Table 1. Errors associated with analyses are approximately 0.02 for Na_2O, MgO, Ti_2O, FeO; 0.08 for Al_2O_3 and CaO; 0.05 for SiO_2; and 0.04 for V_2O_3.[a] *Continued.*

Sample #	Phase	Na_2O	MgO	Al_2O_3	SiO_2	CaO	TiO_2	FeO	V_2O_3	Totals
sp21	Mel	bd	5.03	24.05	29.75	41.50	bd	bd	bd	100.33
sp22	Mel	bd	4.74	24.71	29.40	41.61	bd	bd	bd	100.46
sp23	Mel	bd	5.06	23.89	29.93	41.69	bd	bd	bd	100.57
sp24	Mel	bd	5.23	23.57	30.10	41.66	bd	bd	bd	100.56
sp25	Mel	bd	4.76	24.65	29.24	41.59	bd	bd	bd	100.24
Edge 3										
sp1	Mel	bd	3.38	27.99	27.16	41.54	bd	bd	bd	100.07
sp2	Mel	bd	3.53	28.04	27.44	41.90	bd	bd	bd	100.91
sp3	Mel	bd	4.55	25.08	29.13	41.80	bd	bd	bd	100.56
sp4	Mel	bd	4.86	24.43	29.53	41.60	bd	bd	bd	100.42
sp5	Mel	bd	4.71	24.85	29.39	41.76	bd	bd	bd	100.71
sp6	Mel	bd	3.91	26.84	28.17	41.63	bd	bd	bd	100.55
sp7	Mel	bd	5.37	22.79	30.29	41.44	bd	0.19	bd	100.08
sp8	Mel	bd	5.58	22.70	30.47	41.50	bd	0.12	bd	100.37
sp9	Mel	bd	4.88	24.41	29.54	41.85	bd	bd	bd	100.68
sp10	Mel	bd	4.66	24.91	29.16	41.69	bd	bd	bd	100.42
sp11	Mel	bd	5.64	22.34	30.81	41.70	bd	bd	bd	100.49
sp12	Mel	bd	5.70	21.77	31.11	41.84	bd	0.13	bd	100.55
sp13	Mel	bd	5.37	22.63	30.38	41.62	bd	bd	bd	100.00
sp14	Mel	bd	5.24	23.15	30.30	41.85	bd	bd	bd	100.54
sp15	Mel	bd	5.44	22.49	30.52	41.77	bd	0.15	bd	100.37
sp16	Mel	bd	5.50	22.43	30.74	41.70	bd	bd	bd	100.37
sp17	Mel	0.05	6.86	19.08	32.68	41.57	bd	bd	bd	100.19
sp18	Mel	bd	4.13	26.35	28.33	41.78	bd	bd	bd	100.59
sp19	Mel	bd	4.25	26.06	28.70	41.86	bd	bd	bd	100.87
Middle 1										
sp1	Mel	bd	5.60	22.01	30.73	41.94	bd	bd	bd	100.28
sp3	Mel	bd	8.07	18.40	32.60	40.47	bd	0.17	bd	99.71
sp4	Mel	bd	6.18	20.05	31.63	41.55	bd	bd	bd	99.41
sp5	Mel	bd	4.68	23.80	29.44	41.75	bd	bd	bd	99.67
sp6	Mel	bd	5.00	22.67	29.80	41.41	bd	bd	bd	98.88
sp9	Mel	bd	5.10	22.34	29.81	41.43	bd	bd	bd	98.68
sp11	Mel	bd	4.97	23.25	29.90	41.61	bd	bd	bd	99.73
sp12	Mel	bd	7.01	24.36	29.82	36.81	1.56	bd	bd	99.56
sp13	Mel	0.17	7.31	16.85	33.74	41.15	bd	bd	bd	99.22
sp14	Mel	0.07	6.82	17.70	32.65	41.28	bd	bd	bd	98.52
sp15	Mel	bd	4.06	25.04	28.28	41.48	bd	bd	bd	98.86
sp16	Mel	bd	4.51	24.01	28.95	41.65	bd	bd	bd	99.12
sp17	Mel	0.11	7.70	18.52	32.45	40.22	bd	bd	bd	99.00
sp18	Mel	bd	4.14	24.46	28.38	41.42	bd	bd	bd	98.40
sp20	Mel	bd	3.98	25.14	28.01	41.45	bd	bd	bd	98.58
sp21	Mel	bd	5.01	22.73	29.92	41.75	bd	bd	bd	99.41
sp22	Mel	bd	6.85	18.05	32.94	41.60	bd	bd	bd	99.44
sp23	Mel	bd	4.15	25.47	28.60	41.86	bd	bd	bd	100.08
sp24	Mel	0.03	4.90	23.37	29.72	41.74	bd	bd	bd	99.76
sp25	Mel	0.08	5.00	22.84	29.71	41.59	bd	bd	bd	99.22
Middle 2										
sp1	Mel	0.13	7.66	17.04	34.02	41.25	bd	0.12	bd	100.22
sp2	Mel	0.19	8.95	13.36	35.72	40.75	bd	bd	bd	98.97
sp3	Mel	0.18	8.69	13.96	35.95	41.07	bd	0.31	bd	100.16
sp5	Mel	0.20	8.42	14.46	35.57	41.14	bd	0.19	bd	99.98
sp6	Cpx	NA	8.18	18.83	36.68	24.93	11.04	bd	0.65	100.31
sp7	Mel	0.19	8.54	14.46	35.62	41.12	bd	bd	bd	99.93

Table 2. Election microprobe analyses (reported as wt%) of host silicate compositions for spinels listed in Table 1. Errors associated with analyses are approximately 0.02 for Na_2O, MgO, Ti_2O, FeO; 0.08 for Al_2O_3 and CaO; 0.05 for SiO_2; and 0.04 for V_2O_3.[a] *Continued.*

Sample #	Phase	Na_2O	MgO	Al_2O_3	SiO_2	CaO	TiO_2	FeO	V_2O_3	Totals
sp8	Mel	0.12	8.42	14.40	35.51	41.32	bd	bd	bd	99.77
sp9, 10	Mel	0.05	7.64	16.64	34.32	41.47	bd	bd	bd	100.12
sp11	Mel	0.07	6.82	18.59	33.00	41.37	bd	bd	bd	99.85
sp12	Mel	0.15	8.37	14.81	35.37	41.08	bd	bd	bd	99.78
sp13	Mel	0.15	8.54	14.45	35.66	41.42	bd	bd	bd	100.22
sp14, 15	Mel	0.09	8.77	13.84	35.91	40.80	bd	bd	bd	99.41
sp16	Mel	0.09	8.71	13.94	36.11	41.57	bd	bd	bd	100.42
sp17	Mel	0.09	8.06	15.90	34.77	41.13	bd	bd	bd	99.95
sp18	Mel	0.11	8.71	13.85	35.97	41.14	bd	bd	bd	99.78
sp19	Cpx	NA	8.06	19.08	36.35	24.88	11.07	bd	0.67	100.11
sp20	Cpx	NA	9.80	18.49	39.88	25.50	6.87	bd	0.20	100.74
sp21	Cpx	NA	9.45	16.55	39.26	24.96	9.77	bd	0.60	100.59
sp22	Cpx	NA	9.43	19.04	39.06	25.34	7.12	bd	0.20	100.19
sp23	Cpx	NA	10.25	15.90	40.62	25.34	8.26	bd	0.42	100.79
sp25, 26	Cpx	NA	9.93	19.06	40.26	25.55	5.43	bd	0.12	100.35
sp27	Cpx	NA	9.83	19.06	39.33	25.39	6.44	bd	0.20	100.25
sp29	Cpx	NA	9.86	16.37	39.81	25.15	9.06	bd	0.48	100.73
sp35	Cpx	NA	9.61	18.86	39.30	25.31	6.83	bd	0.21	100.12
sp39, 40	Cpx	NA	8.36	18.78	37.11	24.89	10.64	bd	0.57	100.35
sp41	Cpx	NA	7.54	18.82	35.93	24.88	12.55	0.11	0.57	100.40
sp42, 43	Cpx	NA	8.79	17.04	38.09	24.93	10.54	0.02	0.59	100.00
Center 1										
sp1	Cpx	NA	8.87	19.03	38.04	25.29	9.31	bd	0.31	100.85
sp2	Cpx	NA	10.22	15.96	40.68	25.39	8.21	bd	0.31	100.77
sp3	Cpx	NA	8.89	19.05	38.14	25.30	9.08	bd	0.30	100.76
sp4	Cpx	NA	9.86	18.16	39.90	25.71	7.36	0.13	0.21	101.33
sp5	Cpx	NA	9.61	19.73	39.74	25.55	6.49	bd	0.12	101.24
sp6	Cpx	NA	9.61	19.47	39.87	25.64	6.61	bd	0.12	101.32
sp7	Cpx	NA	11.00	15.84	42.55	25.70	6.00	bd	0.11	101.20
sp8	Cpx	NA	8.88	19.02	38.05	25.37	9.30	bd	0.35	100.97
sp9	Cpx	NA	8.75	19.25	38.18	25.40	9.10	bd	0.35	101.03
sp10	Cpx	NA	11.11	15.72	42.74	25.60	5.79	bd	0.12	101.08
sp11	Cpx	NA	10.76	18.69	42.43	25.47	3.69	bd	0.11	101.15
sp12	Cpx	NA	9.19	18.91	39.13	25.57	7.82	bd	0.25	100.87
sp13	Cpx	NA	8.93	18.91	38.27	25.11	8.50	bd	0.18	99.90
sp13	Mel	0.18	9.35	12.51	36.96	41.80	bd	bd	bd	100.80
sp15	Cpx	NA	15.28	34.80	26.93	17.91	7.63	bd	0.52	103.07
sp16	Mel	0.17	9.15	12.10	36.76	41.96	bd	bd	bd	100.14
sp17	Cpx	NA	11.18	15.68	42.54	25.78	6.14	bd	0.13	101.45
sp18	Mel	0.16	8.80	14.01	35.93	41.35	bd	bd	bd	100.09
sp19	Mel-alt	0.10	7.49	21.32	32.17	35.89	2.03	bd	0.21	99.21
sp20	Mel	0.16	8.83	13.72	36.42	41.76	bd	bd	bd	101.05
sp21	Mel	0.16	9.26	12.63	36.92	41.60	bd	bd	bd	100.57
sp22	Mel	0.16	7.66	16.34	34.00	41.30	bd	bd	bd	99.46
sp23	Mel	0.06	7.69	16.93	34.06	41.41	bd	bd	bd	100.15
sp24	Mel	0.12	8.14	15.77	35.06	41.93	bd	bd	bd	101.02
sp25	Mel	0.14	8.76	13.92	35.92	41.57	bd	bd	bd	100.31
sp26	Mel	0.11	7.68	15.46	33.76	40.82	bd	0.12	bd	97.95
sp27	Mel	0.08	7.83	16.83	34.40	41.76	bd	bd	bd	100.90
sp28	Mel	0.18	9.47	12.04	37.25	41.74	bd	bd	bd	100.68
sp30	Mel	0.10	8.55	14.05	35.56	41.56	bd	bd	bd	99.82
sp31	Mel	0.18	9.04	13.97	35.71	41.36	bd	bd	bd	100.26
sp32	Mel	0.15	8.90	13.35	36.16	41.77	bd	bd	bd	100.33
sp33	Mel	0.16	8.90	13.45	36.11	41.59	bd	bd	bd	100.21

Table 2. Election microprobe analyses (reported as wt%) of host silicate compositions for spinels listed in Table 1. Errors associated with analyses are approximately 0.02 for Na_2O, MgO, Ti_2O, FeO; 0.08 for Al_2O_3 and CaO; 0.05 for SiO_2; and 0.04 for V_2O_3.[a] *Continued.*

Sample #	Phase	Na_2O	MgO	Al_2O_3	SiO_2	CaO	TiO_2	FeO	V_2O_3	Totals
Center 2										
sp1	Mel	0.16	8.69	14.48	35.69	41.46	bd	bd	bd	100.48
sp2	An	0.03	0.04	36.56	42.96	20.26	bd	bd	bd	99.85
sp3	Cpx	bd	11.50	17.59	43.72	25.85	2.08	bd	bd	100.74
sp3	Mel	0.18	8.30	15.68	35.20	41.26	bd	bd	bd	100.62
sp4, 5	Cpx	NA	9.86	19.47	39.78	25.35	5.52	bd	0.09	100.07
sp6	Cpx	NA	9.56	19.90	39.49	25.56	5.88	bd	0.10	100.49
sp7	Mel	0.16	8.30	15.28	35.30	40.91	bd	bd	bd	99.95
sp8	Mel	0.18	8.78	13.89	36.03	40.93	bd	0.24	bd	100.05
sp9	Cpx	NA	11.19	16.73	43.24	25.67	3.80	bd	0.16	100.79
sp10, 11	Mel	0.15	8.98	14.17	35.76	40.82	bd	bd	bd	99.88
sp12	Cpx	NA	9.62	18.03	39.97	25.23	7.22	bd	0.41	100.48
sp13	Mel	0.15	7.36	17.99	33.68	41.32	bd	bd	bd	100.50
sp14	Mel	0.16	7.29	19.03	33.20	36.93	0.06	0.94	bd	97.61
sp15, 16	Cpx	NA	11.25	15.43	42.42	25.47	5.14	bd	0.15	99.86
sp17	Cpx	NA	9.86	16.22	39.30	25.02	9.68	bd	0.49	100.57
sp18	Cpx	NA	10.42	15.88	40.40	25.31	7.94	bd	0.29	100.24
sp19	Cpx	NA	9.55	18.67	39.07	25.24	7.96	bd	0.21	100.70
sp20	Cpx	NA	9.38	18.44	38.75	25.12	7.81	bd	0.23	99.73
sp21	Cpx	NA	11.33	15.36	42.21	25.29	5.70	bd	0.16	100.05
sp22, 23	Cpx	NA	10.10	16.83	40.68	25.12	6.98	bd	0.37	100.08
sp25	Mel	bd	9.96	11.35	37.74	41.16	bd	bd	bd	100.21
sp27	Cpx	NA	13.12	12.70	46.35	25.47	2.82	bd	0.05	100.51
sp26	Cpx	NA	13.25	12.40	46.03	25.27	2.79	bd	bd	99.74
sp27	Cpx	NA	13.13	12.62	46.29	25.38	2.96	bd	bd	100.38
sp30	Mel	0.18	9.85	12.48	36.57	40.44	bd	bd	bd	99.52
Center 3										
sp1	Cpx	NA	8.83	17.16	37.90	25.21	10.52	bd	0.56	100.18
sp2	Cpx	NA	8.95	18.66	38.03	25.33	9.01	bd	0.32	100.30
sp3	Cpx	NA	9.86	19.15	39.90	25.46	5.81	bd	0.08	100.26
sp4	Cpx	NA	7.98	18.93	36.42	24.87	11.45	bd	0.54	100.19
sp5	Cpx	NA	9.08	16.74	38.48	25.18	10.53	bd	0.60	100.61
sp6	Cpx	NA	10.82	15.91	41.55	25.43	6.74	bd	0.20	100.65
sp7	Cpx	NA	8.98	19.03	38.27	25.32	8.25	bd	0.31	100.16
sp8	Cpx	NA	9.51	19.71	39.55	25.35	5.81	bd	0.11	100.04
sp9	Cpx	NA	9.47	18.26	39.86	25.46	7.53	bd	0.35	100.93
sp10	Cpx	NA	11.20	15.88	42.79	25.65	4.87	bd	0.09	100.48
sp10	Mel	0.12	7.24	17.84	33.68	41.29	bd	0.24	bd	100.41
sp11	Mel	0.13	7.41	17.27	33.91	41.33	bd	0.21	bd	100.26
sp12	Mel	0.17	7.92	15.97	34.48	40.86	bd	bd	bd	99.40
sp13	An	bd	0.11	36.40	42.95	20.26	bd	bd	bd	99.72
sp14	Mel-alt	bd	16.41	7.38	38.61	36.92	bd	1.04	bd	100.36
sp16	Mel	bd	7.43	17.60	33.78	41.46	bd	bd	bd	100.27
sp17	Mel	0.13	7.71	16.58	34.27	41.30	bd	0.15	bd	100.14
sp18	Mel-alt	0.05	7.39	16.90	33.66	36.10	bd	4.56	0.04	98.70
sp19	Cpx	NA	11.16	17.30	43.26	25.66	2.88	bd	0.21	100.47
sp19	Mel-alt	0.02	9.87	13.80	37.53	34.16	0.08	4.11	bd	99.57
sp20	Cpx	NA	10.27	18.27	40.70	25.45	5.69	bd	0.14	100.52
sp21	Mel	0.14	7.33	17.83	33.61	41.45	bd	bd	bd	100.36
sp22	Mel	0.15	7.69	17.09	34.11	41.54	bd	0.00	bd	100.58
sp23	Cpx	NA	9.25	18.73	38.59	25.16	8.08	0.00	0.28	100.09

[a]Mel = melilite; Mel-alt = melilite that shows clear textural, EDS evidence for alteration; Cpx = Clinopyrxene (often called fassaite); An = anorthite; NA = not analyzed; bd = below detection limit.

Table 3. Spinel minor element chemistry (wt%) and their oxygen isotopic compositions. Analytical uncertainties associated with the data are approximately ±0.02 for Ca, Ti, V, and Cr; and ±0.03 for Fe.[a]

Sample	Host	Ca	Ti	V	Cr	Fe	$\delta^{18}O$ (‰)	$\delta^{17}O$ (‰)	$\Delta^{17}O$ (‰)
Edge 3									
sp1v	Mel	0.60	0.34	0.54	0.11	0.04	–50.5 ± 1.6	–50.7 ± 1.7	–24.4 ± 1.2
sp2v	Mel	0.50	0.36	0.60	0.10	0.20	–49.3 ± 1.6	–50.6 ± 1.7	–24.9 ± 1.2
sp18	Mel	0.60	0.38	0.89	0.20	0.16	–51.9 ± 1.5	–52.2 ± 1.7	–25.2 ± 1.2
Center 3									
sp2	Cpx	bd	0.54	0.27	0.09	0.04	–52.0 ± 1.6	–54.0 ± 1.6	–26.9 ± 1.1
sp2–2	Cpx	bd	0.54	0.27	0.09	0.04	–50.9 ± 1.7	–51.9 ± 1.8	–25.4 ± 1.4
sp3	Cpx	bd	0.48	0.25	0.09	0.03	–48.3 ± 1.6	–50.3 ± 1.7	–25.2 ± 1.2
sp11a	Mel	bd	0.18	0.18	0.09	0.25	–48.8 ± 1.7	–50.5 ± 1.7	–25.1 ± 1.2
sp16a	Mel	bd	0.20	0.22	0.10	0.04	–48.1 ± 1.8	–49.3 ± 1.7	–24.3 ± 1.3

[a]a = Spinel is within 100 μm of an alteration zone within melilite; v = Spinel is within 100 μm of a vein of alteration; Mel = melilite; Cpx = clinpyroxne (often called by an unoffical name of fassaite).

Table 4. List of silicate major element chemistry (wt%) and their oxygen isotopic compositions. Errors associated with analyses of silicates are approximately 0.02 for Na_2O, MgO, Ti_2O, FeO; 0.08 for Al_2O_3 and CaO; 0.05 for SiO_2; and 0.04 for V_2O_3.[a]

Sample #	Phase	Na_2O	MgO	Al_2O_3	SiO_2	CaO	TiO_2	FeO	V_2O_3	Total	$\delta^{18}O$ (‰)	$\delta^{17}O$ (‰)	$\Delta^{17}O$ (‰)
Edge 3													
All spinels	Mel	bd	3.38	27.99	27.16	41.54	0.10	0.02	bd	100.27	–0.9 ± 1.5	–3.9 ± 1.7	–3.5 ± 1.1
Center 3													
Sp 2, 3	Cpx	bd	9.86	19.15	39.90	25.46	5.81	0.02	0.08	100.38	–40.8 ± 1.6	–44.2 ± 1.8	–23.1 ± 1.3
Sp 11, 16	Mel	0.13	7.41	17.27	33.91	41.33	0.02	0.21	bd	100.35	1.9 ± 1.6	–3.0 ± 1.7	–3.9 ± 1.2

[a]Mel = melilite; Cpx = clinopyroxene (often called by an unoffical name of fassaite).

cools, this new liquid will crystallize spinel + clinopyroxene first, then when the composition evolves to the cotectic line, melilite will begin to crystallize until finally the invariant point is achieved and anorthite crystallizes.

Interpretation of Spinel Inclusions in Clinopyroxene

The above re-melting model qualitatively explains the correlations between the Ti and V concentrations for spinel inclusions in clinopyroxene and the Ti and V concentrations in the surrounding clinopyroxene (Figs. 8 and 9). Ti and V are compatible elements in clinopyroxene, thus the concentrations of these elements in the liquid will decrease with increasing crystallization. This will produce strong core-enriched zoning in clinopyroxene, as is well documented (e.g., Simon, Grossman, and Davis 1991). Assuming that spinels are included in clinopyroxene almost as fast as they form, the Ti and V concentrations in spinel co-crystallizing with clinopyroxene will decrease in a correlated way, qualitatively accounting for the observed trends. Thus, on Fig. 1c and the equivalent figures in Connolly and Burnett (1999), the first crystallized spinels in the liquid produced by re-melting are found as inclusions in clinopyroxene and have the highest Ti and V contents. This interpretation assumes that a spinel inclusion and the surrounding clinopyroxene co-crystallized from the same liquid. This assumption can also explain the overall fine spinel grain size: spinels are gobbled up as inclusions in clinopyroxene (and later melilite) as fast as they are formed. The large spinels, which are an exception to this assumption, within TS-34 are discussed below.

Modeling (Ti, V) Systematics for Spinel Inclusions in Clinopyroxene

Although the re-melting hypothesis can qualitatively account for the (Ti, V) systematics, a significant test is whether a quantitative description is also possible. The details are complex and given in Appendix A. We summarize the major conclusions here. The unique features of the data that must be accounted for by the re-melting hypothesis are the trends for spinel inclusions in clinopyroxene (Figs. 8 and 9).

Although there are uncertain parameters that can be varied, we are able to model successfully the "centers of gravity" of the Ti trends for both TS-34 and Leoville 3537–2 (Figs. A1–A3) with reasonable parameter choices (Tables A1–A3), following the partitioning of Ti^{+3} and Ti^{+4} separately. An especially significant success is that both the TS-34 and Leoville 3537–2 data can be described with the same set of clinopyroxene crystal-liquid partition coefficients for Ti, despite the fact that Leoville appears to have a significantly lower bulk Ti concentration than TS-34. One serious problem, common to all apparently successful models, is that most of the spinel inclusions in clinopyroxene should have relatively low Ti concentrations (<0.3%), but this is not observed.

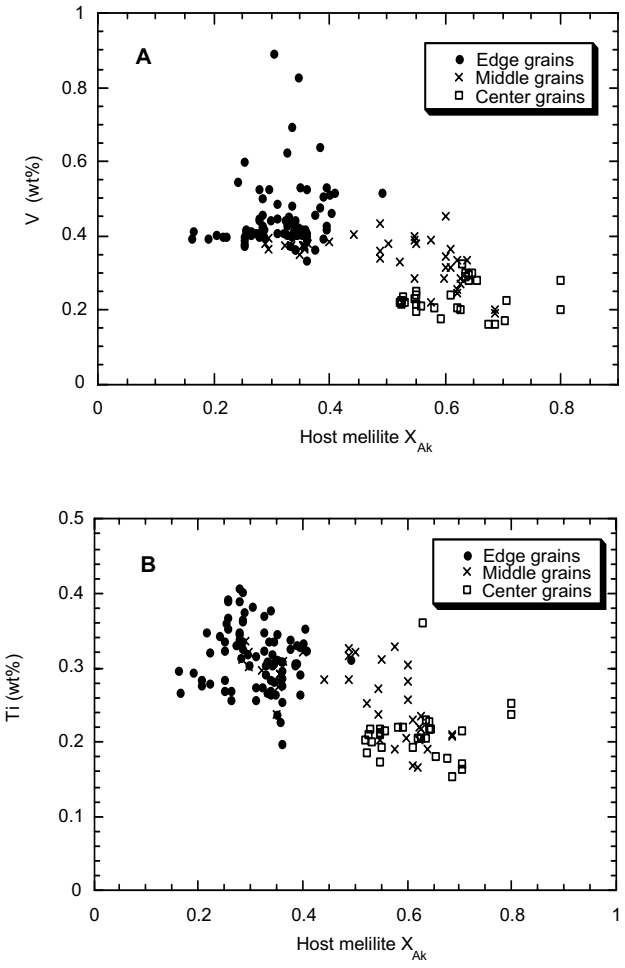

Fig. 5. a) Plot of V concentrations of spinels to $X_{Åk}$ of their respected host melilites from TS-34; b) Plot of Ti concentrations of spinels to $X_{Åk}$ of their host melilites. Here, an almost bimodal distribution is observed with the break at ~$X_{Åk}$ = 0.45. The trend of crystallization for each plot is from left to right: increases in $X_{Åk}$ represent increased crystallization of melilite. In grains with $X_{Åk}$ >0.45, there is a hint of an inverse correlation of V and Ti with $X_{Åk}$, as would be expected for co-crystallizing spinel, melilite, and clinopyroxene. The error associated with each analysis is approximately the same size as the symbols. If error bars are plotted, many of the differences between data points become obscured, thus we have not shown these.

The V trends for spinel inclusions in clinopyroxene (Figs. 8 and 9) are especially difficult to model by fractional crystallization because the V in clinopyroxene varies by over a factor of 10, while the V in presumably co-crystallizing spinel varies by only a factor of 2–3. No solutions were found for single V crystal-liquid partition coefficients in spinel and clinopyroxene (i.e., ignoring the possible presence of V^{+3} and V^{+2}). There are few constraints on multiple valence state models; but surprisingly, we are also unable to fit the V data for spinel inclusions in clinopyroxene with reasonable parameter choices if constant partition coefficients are assumed for V^{+3} and V^{+2}. Overall, we regard the results of our simple models as unsatisfactory. This may mean that the re-melting hypothesis is wrong or that, more likely, our models are too simplistic in assuming constant partition coefficients, modal crystallization, etc.

Interpretation of Spinel Inclusions in Melilite

Further evidence for the re-melting hypothesis is provided by the V and Ti contents of spinel referenced to the host melilite $X_{Åk}$. Inspection of Figs. 5–7 shows that there is an apparently bimodal distribution of melilite composition accompanied by significant changes in spinel composition above and below approximately $X_{Åk}$ ~0.45. With one exception, there are no spinels within melilite between $X_{Åk}$ 0.4 and 0.5 for TS-34. Given the size of the TS-34 data set, it is unlikely that we failed to sample spinels in this range of $X_{Åk}$. Consistent with Beckett, Simon, and Stolper (2000), we interpret this composition as the boundary between two populations of melilite: the initial population and the population that crystallized after re-melting.

Although there is some overlap, the spinel V and Ti concentrations tend to be systematically lower at $X_{Åk}$ >0.45 (Figs. 5–7). These data define an almost bimodal distribution of Ti or V with $X_{Åk}$, most pronounced with the center grains. Although there is considerable scatter, the TS-34 V data (Fig. 5a) are consistent with the pattern expected for our re-melting model: no correlation between V and $X_{Åk}$ up to $X_{Åk}$ = 0.4, changing to a negative correlation with $X_{Åk}$ greater than 0.45. The V data for the other inclusions (Figs. 6 and 7) are consistent with the same trend and have less scatter for $X_{Åk}$ >0.45; however, there are fewer data. A similar inverse correlation of Ti and $X_{Åk}$ for $X_{Åk}$ >0.45 is present in Figs. 6 and 7, but is not clear in the TS-34 data (Fig. 5).

Subsolidus Increases in Ti and V in Spinels

An alternative to the re-melting model is that the distributions of Ti and V in spinel are due to local subsolidus re-equilibration between spinel and clinopyroxene or between spinel and melilite. The correlation between Ti in spinel inclusions to host clinopyroxene Ti content is suggestive of subsolidus reactions and was so interpreted by Meeker, Wasserburg, and Armstrong (1983), who first reported this trend.

The local re-equilibration hypothesis is made plausible by experiments (Connolly and Burnett 2001) in the spinel + CAI liquid field showing that both Ti and V in spinel rapidly equilibrate with the liquid (100 hours or less) by diffusion. These data are suggestive, but apply only indirectly to the issue of subsolidus re-equilibration in actual type B CAIs because re-equilibration would here occur at a much lower temperature and because the host phase (clinopyroxene or melilite) must co-operate in enabling the re-equilibration.

Re-Equilibration of Spinel Inclusions in Clinopyroxene.

The data in Figs. 8 and 9 are reasonably consistent with a

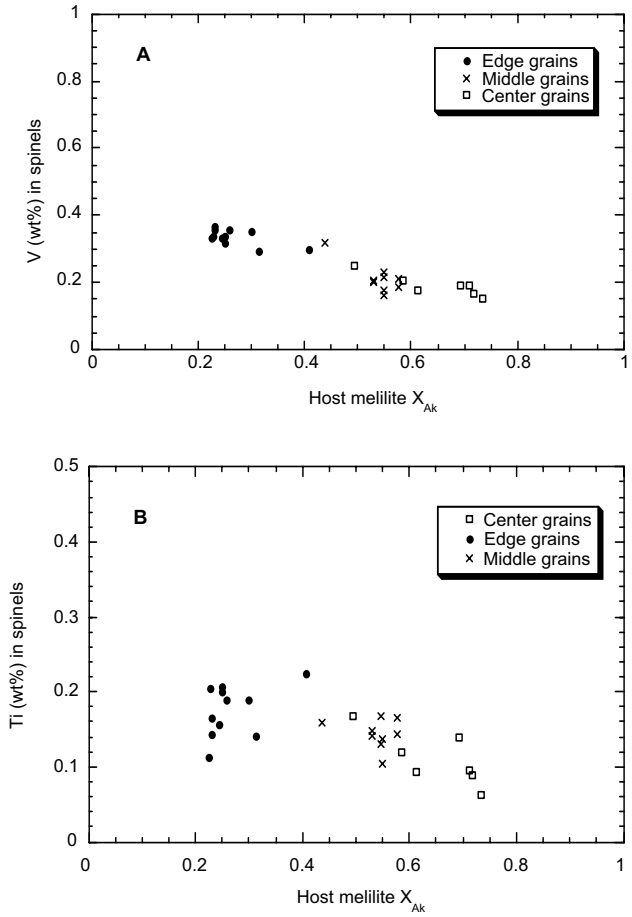

Fig. 6. a) Plot of V concentrations of spinels to $X_{Åk}$ of their respected host melilites from Leoville 3537–2; b) Plot of Ti concentrations of spinels to $X_{Åk}$ of their host melilites for Leoville 3537–2. Here, an almost bimodal distribution is observed with the break at ~$X_{Åk}$ = 0.45. The trend of crystallization for each plot is from left to right: increases in $X_{Åk}$ represent increased crystallization of melilite. In grains with $X_{Åk}$ >0.45, there is a hint of an inverse correlation of V and Ti with $X_{Åk}$, as would be expected for co-crystallizing spinel, melilite, and clinopyroxene. The error associated with each analysis is approximately the same size as the symbols. If error bars are plotted, many of the differences between data points become obscured, thus we have not shown these.

constant Ti spinel/clinopyroxene partitioning ratio of about 0.07 for both inclusions, plausible for subsolidus re-equilibration. The few analyses of spinel inclusions and adjacent clinopyroxene available for TS-23 (Connolly and Burnett 1999), and the data of Meeker, Wasserburg, and Armstrong (1983) are also consistent with this ratio.

One complication is that the Ti^{+3}/Ti^{+4} ratio in type B CAI clinopyroxenes decreases from core to rim (e.g., Simon, Grossman, and Davis 1991), implying that a constant partitioning ratio should not be observed. It may be that there is an underlying curvature to the basic trend on Figs. 8 and 9 that is lost in the overall scatter.

To understand why the highest spinel Ti concentrations are observed for spinel inclusions in clinopyroxene (Fig. 1c and equivalent figures in Connolly and Burnett 1999), Ti is required to diffuse from clinopyroxene to spinel. But, because Ti concentrations are much larger in clinopyroxene than spinel, the distances and amounts of Ti required would not produce any significant effect on the clinopyroxene Ti zoning. We conclude that the re-equilibration hypothesis explains the Ti data for spinel inclusions in clinopyroxene well.

The V correlations on Figs. 8 and 9 do not correspond to a constant partition coefficient. V in the clinopyroxene varies by at least a factor of 10, whereas V in spinel varies by a factor of 2–3. The simplest possible explanation is that the V trends in Figs. 8 and 9 are due to fractional crystallization following re-melting. However, the V correlations on Figs. 8 and 9 can also be explained by partial re-equilibration, i.e., systematic deviations from complete re-equilibration because of the inability of the clinopyroxene to supply V to the spinel.

In a partial re-equilibration model for V, early crystallizing spinels are incorporated as inclusions in clinopyroxene and re-equilibrated. For partial re-equilibration, unlike the Ti case of complete re-equilibration, quantitative interpretation requires knowledge of the initial V of spinel inclusions after re-melting but prior to subsolidus heating. Although these concentrations are not known with confidence, we can make a reasonable assumption that the early-formed spinels had V concentrations of 0.15–0.2 wt% prior to re-equilibration, uncorrelated with pyroxene composition. If this is true, the spinel/clinopyroxene partition coefficient for V is greater than 10, requiring V to have moved from clinopyroxene to spinel in an attempt to reach equilibrium partitioning. Thus, spinels with the lowest V are the closest to equilibrium. This model, including the assumed 0.15–2 wt% initial V in spinel prior to re-equilibration, appears to hold for both Leoville 3537–2 and TS-34. However, this specific model is illustrative, not unique. Summarizing, partial re-equilibration can explain the V trends on Figs. 8 and 9.

Re-Equilibration of Spinel Inclusions in Melilite

The data for V and Ti for spinels enclosed by melilite are more difficult to explain by subsolidus re-equilibration. We are required to explain the full range of V and Ti concentrations on Fig. 1b, assuming that the subsolidus re-equilibration was the last event in the history of these materials.

V is a trace element in melilite. Our electron probe data set an upper limit of 0.01 wt% for V in melilite. Assuming a solar V/Ti and all V^{+3}, we estimate the order of 10 ppm for TS-34 based on partition coefficient systematics from Beckett et al. (1990) and the bulk Ti for TS-34 from Beckett (1986). Ti concentrations in TS-23 melilite are 0.01–0.015 wt%, and are correlated with $X_{Åk}$ (Johnson, Burnett, and Woolum 1988).

The critical issue here is the directions V and Ti have to

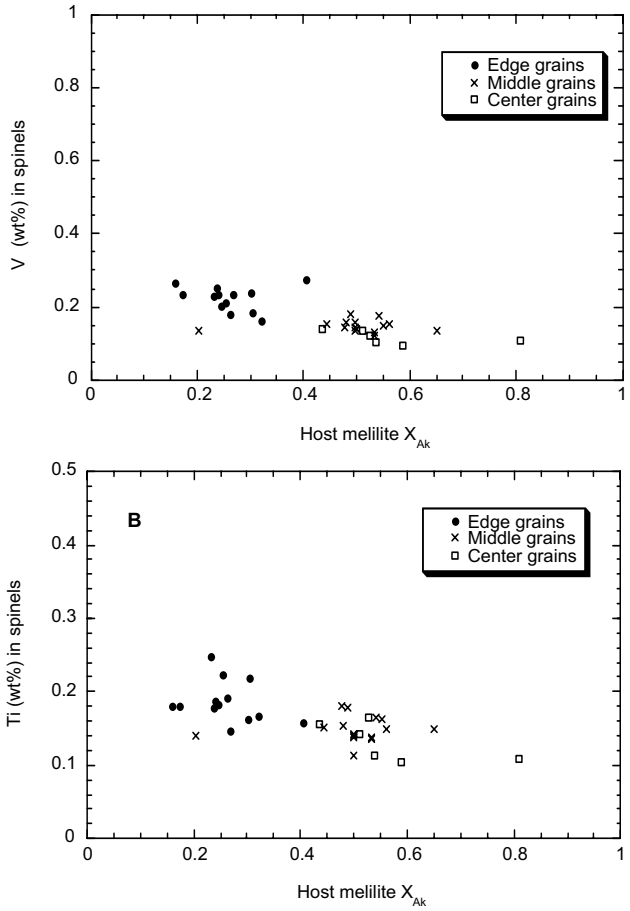

Fig. 7. a) Plot of V concentrations of spinels to XÅk of their respected host melilites from Allende TS-23; b) Plot of Ti concentrations of spinels to XÅk of their host melilites for Allende TS-23. Here an almost bimodal distribution is observed with the break at ~$X_{Åk}$ = 0.45. The trend of crystallization for each plot is from left to right: increases in $X_{Åk}$ represent increased crystallization of melilite. In grains with $X_{Åk}$ >0.45, there is a hint of an inverse correlation of V and Ti with $X_{Åk}$, as would be expected for co-crystallizing spinel, melilite and clinopyroxene. Error associated with each analysis is approximately the same size as the symbols. If errors bars are plotted many of the differences between data points become obscured, thus we have not shown these.

move to approach equilibrium partitioning. V and Ti are much more compatible in spinel than melilite. Nevertheless, a high (V, Ti) spinel included in melilite may have more V and/or Ti than required for equilibrium partitioning with melilite. Thus, equilibration may require V and/or Ti to move from spinel to melilite. Or, the opposite may be true. Further, V might behave differently from Ti.

If re-equilibration requires V and/or Ti to move from melilite to spinel, this would seem difficult, given the low Ti, and especially V, concentrations in melilite . In contrast, loss of V and/or Ti from spinel to melilite is easier, but might eventually be limited by slow diffusion in melilite. Some limits on diffusion of V and Ti in melilite are set by the observed major element zoning, but V and/or Ti diffusion might be much faster than the coupled Al-Si diffusion required for $X_{Åk}$ homogenization. Consequently, diffusion of V and/or Ti from over hundreds of microns in melilite cannot be ruled out, but we suggest it is unlikely.

In the absence of relevant diffusion data, any conclusions must be based on the systematics of the data themselves. In contrast to the data for spinel inclusions in clinopyroxene, where the systematics strongly suggested re-equilibration, there is really nothing in the data for spinel inclusions in melilite (Figs. 5–8) that suggests that re-equilibration has had a major effect.

Clearly, V and/or Ti have not been homogenized among spinel inclusions in melilite, thus mm-scale diffusion of V and/or Ti in melilite is unlikely. Consequently, the edge and center (more specifically $X_{Åk}$ above and below 0.45) populations need separate consideration. Within either population, changes in spinel V and/or Ti concentrations of the order of 0.1 wt% relative to some unknown initial distributions would be expected to produce greater homogeneity, or at least better correlations with $X_{Åk}$ than are seen in Figs. 5 to 7. However, for both populations, it may be that the (V, Ti) distributions in spinel prior to subsolidus heating were even broader than today. Alternatively, and probably more likely, the (V, Ti) distributions for spinel inclusions in melilite can be regarded as, essentially, the initial distributions either at the end of the initial crystallization (edge population) or the end of crystallization following re-melting (center populations). Changes of the order of hundreds of ppm are possible, but these produce no changes in interpretations. Well defined correlations of V and/or Ti with melilite composition for $X_{Åk}$ >0.45 may have been present after re-melting, but chaotic aspects in the initial stages of re-equilibration (e.g., inhomogeneities in the melilite V distribution) may have produced the scatter observed in Figs. 5–7.

Accepting this interpretation of spinel inclusions in melilite, we can revisit the above model for the re-equilibration of V in spinel inclusions in clinopyroxene. The initial distribution of V concentrations for the clinopyroxene inclusions is given by what is observed in melilite at present. The data on Figs. 5–7 for inclusions in center melilites generally conform to the 0.15–0.2 wt% V range assumed in the partial re-equilbration model for inclusions in clinopyroxene. There probably was some weak initial correlation of spinel V with clinopyroxene V, but this is compatible with significant V partial re-equilibration of clinopyroxene and included spinels.

Interpretation of Zoning Data

Chemical variations within single spinel grains, or zoning, are potentially diagnostic in discriminating between the two hypotheses. In terms of the re-melting hypothesis, a large spinel grain co-crystallizing with

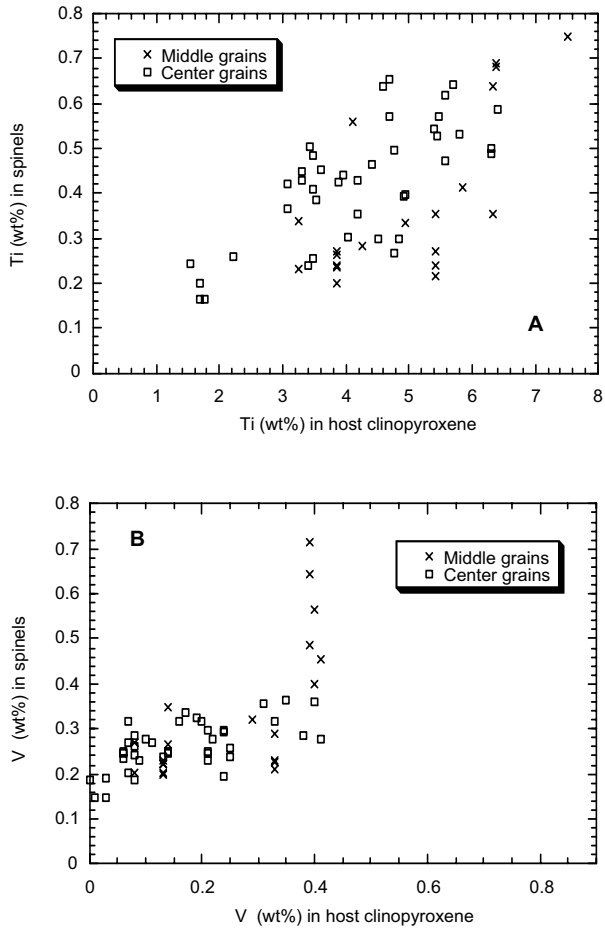

Fig. 8. a) Plot of Ti (wt%) in spinel to the Ti (wt%) of adjacent host clinopyroxene from TS-34. Although there is significant scatter, a positive trend is observed; b) Plot of V (wt%) of spinel to V (wt%) of host clinopyroxene from TS-34 showing a slight positive correlation. The crystallization sequence of clinopyroxene is from right to left with decreasing Ti in clinopyroxene, the first formed having the highest Ti values. The error associated with each analysis is approximately the same size as the symbols. If error bars are plotted, many of the differences between data points become obscured, thus we have not shown these.

clinopyroxene should show enhancements of both Ti and V in the cores. Independent of the (V, Ti) hypotheses, the existence of the large spinel grains in the center regions of TS-34 can be regarded as a consequence of re-melting or multiple re-melting events. An intriguing issue, for which we have no good explanation, is why, out of the three inclusions we investigated, such large spinel grains are found only in TS-34.

In terms of the subsolidus re-equilibration hypothesis, large spinel grains should ideally be homogeneous, but depending on the subsolidus thermal history, could show gradients in either sense depending on whether V and/or Ti were moving in or out of the spinel during re-equilibration. We observe an overall lack of consistent zoning patterns within spinels and this is a problem for the re-equilibration hypothesis. But, the existence of at least one large spinel inclusion in clinopyroxene with relatively homogeneous Ti and V concentrations suggests that Ti and V homogenization in spinel by diffusion would be complete if given the chance. There are several possible reasons for lack of consistent zoning patterns: 1) for spinel grains sharing a boundary with clinopyroxene, local variations in clinopyroxene V and/or Ti concentrations might induce complicated 20–50 micron scale variations in the adjacent spinel; 2) assuming that alteration is prior to, or contemporaneous with, subsolidus re-equilibration, this could result in ultra-thin films on spinel grains that represent varying degrees of permeability of Ti and V flowing in or out of the spinel. This would explain why, overall, correlations have less scatter for Leoville 3537–2 than for TS-34; 3) perhaps internal domains in the spinel crystals are barriers to complete homogenization, etc. These are special pleadings, but they cannot be ruled out. In summary, both hypotheses can reconcile the complicated zoning patterns in the large spinel grains from TS-34, although this is more easily done for the re-melting hypothesis.

Origin of the Scatter in the (Ti, V) Systematics

The above discussion has primarily focused on interpreting the centers of gravity of the observed trends. However, large amounts of scatter are a major feature of all trends and warrant some consideration. As discussed by Connolly and Burnett (2000) and consistant with our discussions within this paper, the overall scatter in Ti and V can be explained by a re-melting hypothesis.

Re-equilibration could also produce the observed scatter. Accepting from above that the trends for spinel inclusions in melilite may not represent re-equilibration, we focus on clinopyroxene. Ti and V diffusion coefficients will vary with clinopyroxene composition, but this should still produce smooth, if uninterpretable, trends. Analogous to the re-melting hypothesis, lack of a well-defined adjacent host phase composition could be a major source of scatter. For V, where only partial re-equilibration is indicated, variations in spinel grain size, will produce scatter, as discussed above. Also, the "real world" effects that would cause "effective" spinel diffusion coefficients to vary or that would impede diffusion to varying degrees, as listed in the zoning discussion above, would also be a source of scatter in general. In summary, the scatter in the various correlations can be explained with both hypotheses.

Constraints from Oxygen Isotope Compositions

The oxygen isotope data (Fig. 10a) are in general agreement with well-established systematics for type B1 CAIs in that spinel is the most ^{16}O-enriched phase, followed

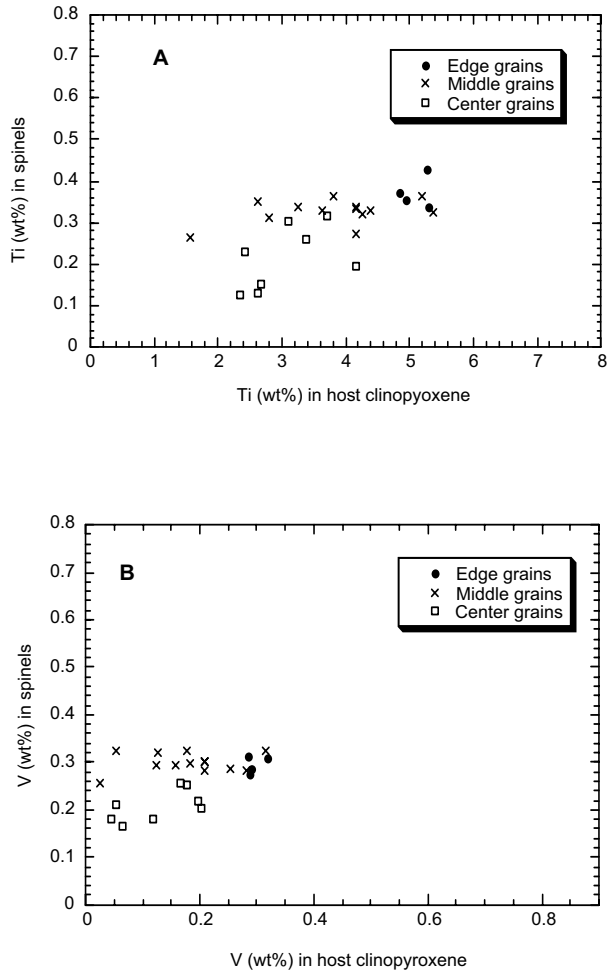

Fig. 9. a) Plot of Ti (wt%) in spinel to the Ti (wt%) of adjacent host clinopyroxene from Leoville 3537–2. Although there is significant scatter, a positive trend is observed; b) Plot of V (wt%) of spinel to V (wt%) of host clinopyroxene in Leoville 3537–2 showing a slight positive correlation. The crystallization sequence of clinopyroxene is from right to left with decreasing Ti in clinopyroxene, the first formed having the highest Ti values. The error associated with each analysis is approximately the same size as the symbols. If error bars are plotted, many of the differences between data points become obscured, thus we have not shown these.

closely by clinopyroxene, with melilite approximately 40‰ less ^{16}O-enriched than pyroxene. The observations are characterized by isotopic homogeneity among different populations of spinel (and melilite) grains, and extreme isotopic heterogeneity between different mineral phases. The widely-accepted interpretation of this pattern is that it results from a sub-solidus oxygen isotopic exchange event(s) with an external reservoir, usually thought to be nebular gas, which increased both δ^{17}O and δ^{18}O values for melilite from the initially low values which are retained in clinopyroxene and spinel (see Clayton 1993 for a discussion). This initial value is normally considered to be ≈–40‰ for both δ^{17}O and δ^{18}O, based on high-precision analyses of mineral separates from both CV and CM chondrites (Clayton et al. 1977; Clayton and Mayeda 1984). However, the spinels analyzed here are clearly ~10‰ more enriched in ^{16}O than this composition (Fig. 10b). In principle, this difference could be due to melilite (or anorthite) impurities in the mineral separates or, alternatively, it could truly reflect multiple spinel populations in a type B CAI. Our data represent the first in situ analyses of specific generations of spinel from the same CAI, and thus provide an opportunity to test this hypothesis. Additionally, the oxygen isotope data provide constraints on the relative timing and nature of any re-melting and/or subsolidus chemical and isotopic exchange events.

The ~5‰ difference in Δ^{17}O values of spinel between the ion microprobe and the mineral separate data of Clayton et al. is unlikely to be due to impurities since that would imply a relatively large amount of contamination that is not supported by the small (~1.5‰) difference in Δ^{17}O between spinel separated from melilite and that separated from pyroxene. Thus, it would appear that the data are best understood as indicating that isotopically distinct populations of spinel exist in TS-34. Although we have not sampled a large number of spinels, restricting the oxygen analyses to only large grains, we have included grains from both the center and edge regions with V and Ti contents varying by factors of 5 and 3, respectively, making it very unlikely that we have missed a significant population of chemically distinct spinels. The fact that they all have essentially the same oxygen isotopic composition, therefore, implies that there do not exist large intrinsic differences in oxygen isotopes based on crystallization sequence, and thus the difference between the mineral separate data and our data (and also a significant number of other ion probe data; see McKeegan and Leshin 2001 for a summary) cannot be explained as us having luckily sampled only primary (or relict) spinels. It could, however, imply that the large population of relatively small spinel grains have experienced a significant amount (>20%) of isotopic exchange. If this interpretation is correct, our data further indicate that this isotopic exchange would have to have occurred following complete spinel crystallization.

The isotope heterogeneity among the different mineral phases also constrains the nature and timing of possible re-melting events. If re-melting had occurred after significant oxygen isotopic exchange, then oxygen isotope compositions would have been essentially homogenized between melilite and clinopyroxene. Additionally, there would be a large fraction of ^{16}O-poor spinel, and this ought to include some of the larger spinel grains. None of these effects are observed, thus re-melting is constrained to have been prior to oxygen isotopic exchange in melilite.

It is also plausible to consider oxygen isotopic exchange with an external reservoir during a partial melting event since oxygen diffusion within the melt is known to be rapid (see Ryerson and McKeegan [1994] for a discussion of oxygen self diffusion rates). Additionally, the crystallization sequence

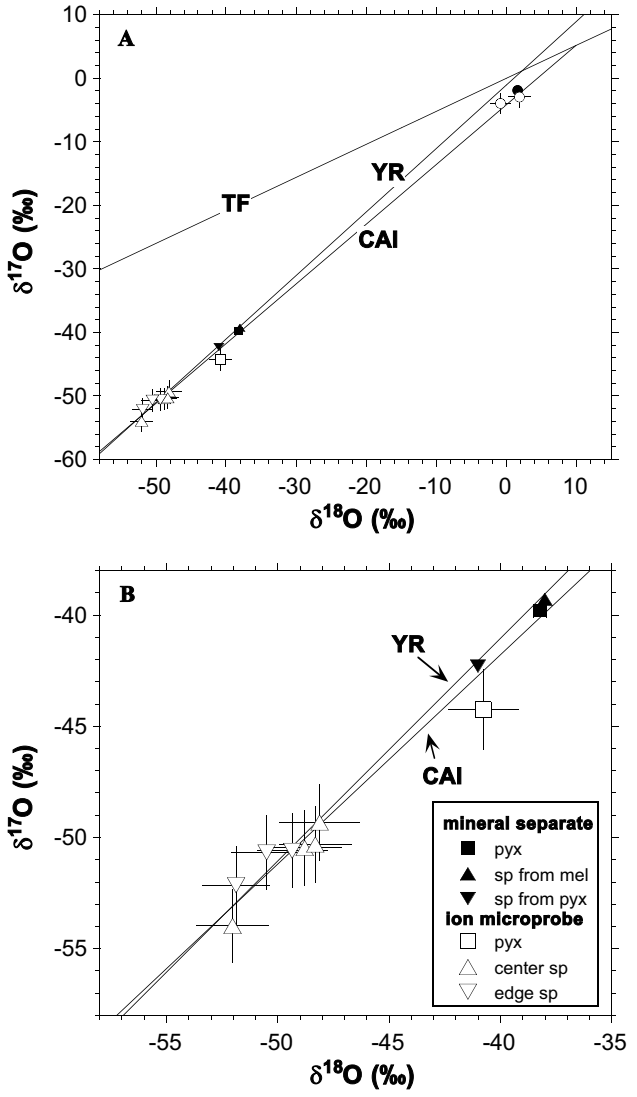

Fig. 10. Oxygen isotope compositions for co-existing phases in Allende TS-34 are plotted as $\delta^{17}O$ and $\delta^{18}O$ relative to SMOW. Filled symbols are data from mineral separate analyses of TS-34 (aka Al3S4) by Clayton et al. (1977). Open symbols (with 1σ error bars) represent in situ analyses from this work. Circles are melilite, squares are pyroxene, triangles are spinel. a) The data fall along the ^{16}O-mixing line of slope 0.94 defined by a least-squares fit to high-precision analyses of Allende CAIs from Clayton et al. (1977). The slope 1.00 mixing line defined by Young and Russell (1998) is shown for reference. The ion probe data generally agree with the mineral separate data, with the exception of spinel which is more ^{16}O-rich, and the overall pattern is typical of type B CAIs. Melilite from edge and center regions are isotopically indistinguishable. b) Expanded view of the ^{16}O-rich region showing that there exists a small range in spinel isotopic compositions, with, however ,essentially complete overlap of oxygen isotopes between spinels from different locations within the CAI. The offset between the in situ and mineral separate analyses of spinel probably reflects a large population of small spinel grains that are less enriched in ^{16}O. Overall, the data are best understood as indicating that subsolidus oxygen isotopic exchange occurred in all phases, to varying degrees, following the last re-melting event. CAI = Allende CAI mixing line. YR = Young and Russell primitive mixing line. TF = terrestrial mass fractionation line.

during cooling after a partial melting event is qualitatively in the correct order (spinel + pyroxene, then melilite, then anorthite) for an initially ^{16}O-rich melt that is exchanging with an ^{16}O-poor gas. However, quantitatively there are problems because some newly formed spinel (e.g., large center grains) should have a modified oxygen isotope composition, but this is not observed. Another serious problem with the notion of oxygen isotopic exchange during re-melting is that our measurements of 2 melilite grains, one from the edge and one presumably late-forming crystal from the central region, are the same within error. If, as we have argued above, the edge crystal survived the last melting event, then even with relatively fast oxygen diffusion rates in melilite, some ^{16}O-rich cores should be preserved (see Fig. 15 of Ryerson and McKeegan 1994). We have not done extensive measurements of melilite in TS-34, and so cannot rule out that there may exist some ^{16}O-rich melilite somewhere in the inclusion. However we view this to be unlikely given the isotopic homogeneity between the two grains sampled. In one Allende CAI, a large step-function change in oxygen isotopic composition that occurs across a single melilite crystal has been explained as due to isotope exchange during a thermal event that caused localized partial melting and recrystallization of the melilite (Yurimoto, Ito, and Nagasawa 1998). However, this appears to be an exceptional case as the growing database from ion microprobe studies indicates that although ^{16}O-rich melilite may be commonplace in many types of CAIs, it is rare in type B CAIs (McKeegan and Leshin 2001, and references therein).

The preponderance of the evidence indicates that oxygen isotopic exchange in TS-34 must have happened after the last melting event, thus requiring a subsolidus mechanism for the isotope exchange. Ryerson and McKeegan (1994) have discussed the problems involved in reconciling simple cooling histories with gas-solid diffusion, in the absence of water, being the operative mechanism. One such problem was that spinel was considered to be essentially completely retentive of its initial oxygen isotopic composition. However, if our face-value interpretation of the mineral separate data is correct and there does exist a population of small spinel grains with $\delta^{18}O$, $\delta^{17}O \geq -35‰$, then this constraint is relaxed. For example, at moderate subsolidus temperatures (~1000ºC), it is possible to achieve ~20% fractional equilibration in spinel grains <10 μm in diameter while completely equilibrating mm-sized melilite grains and causing only ~10% or less exchange in typical pyroxene crystals (Ryerson and McKeegan 1994). However, such a scenario would require heating for several hundred years, which may be too long for models of CAI residence in the inner parts of the solar accretion disk. In principle, this scenario could be tested by analyses of oxygen isotope abundances in ~5 m spinel grains or by measurements of diffusion profiles by high spatial resolution traverses of large spinels (like those analyzed in this work).

The oxygen isotope data constrain the relative timing of

the re-melting event, but do not discriminate between the two alternative interpretations of the (Ti, V) trends. The homogeneity of oxygen isotopic compositions of spinels with different Ti and V contents indicates that these chemical and isotopic tracers are essentially completely decoupled. This means that if the complete equilibration of Ti and partial re-equilibration of V between clinopyroxene and included spinel is achieved by subsolidus diffusion, then this must occur significantly faster than oxygen diffusion. Although pertinent data for V and Ti diffusion in spinel are lacking, this constraint is plausible based on the sluggishness of oxygen self-diffusion in spinel (Ryerson and McKeegan 1994).

To the extent that re-melting is required to explain other CAI features beyond the spinel data discussed here, the above sequence of oxygen isotopic exchange following re-melting provides a general constraint on the origin of type B1 CAIs. In at least some inclusions (MacPherson and Davis 1993), re-melting appears to have occurred after mineralogical alteration. Thus, the alteration and oxygen exchange events appear to be clearly separated, and a sequence established: alteration before oxygen isotopic exchange. Note that this does not preclude a secondary mineralogical alteration, probably involving parent body fluids, affecting CAI chemical and isotopic compositions, especially of melilite (e.g., Young and Russell 1998). However, significant exchange by diffusion in even very small spinel grains at parent body temperatures (e.g., <600ºC) is unlikely (Ryerson and McKeegan 1994), and thus, if such a population of relatively ^{16}O-poor spinel exists, it would indicate that exchange should also have happened at higher temperatures.

The Origins of Edge Spinels

In all inclusions studied, the grains within the melilites' edge areas have high V contents (extending up to >~0.5 wt% for TS-34; Fig. 1) that do not correlate with spinel Ti or with the $X_{Åk}$ contents of host melilites. The edge spinels are small, and oxygen isotopic analysis was not possible.

As a group, these V-rich spinels could have three possible origins: a) they formed during the initial heating cycle, b) they formed under nonequilibrium conditions, and/or c) they are relict grains. We define relict spinel as either a condensate or a grain that formed in a previous generation of igneous CAIs. None of these explanations can be ruled out and, in fact, a combination of all three may be correct. Explanations a and b are intimately related. If heating was quick and did not provide time for complete thermal equilibration and total melting, spinel crystals would have grown during the heating cycle (Stolper and Paque 1986; Paque, private communication). Such spinels would form too quickly for equilibrium or near equilibrium conditions to exist. To give a specific possibility, if the oxygen fugacity was changing during heating, the proportions of the different valence states of Ti, V, and Cr would change, and thus the corresponding D(sp).

Finally, the V-rich grains could be relict. As was discussed earlier, spinel is the liquidus phase of an average type B CAI bulk composition and is the most likely mineral to survive multiple melting events. If relict grains exist, the most likely location for them would be in the first formed melilite, the edge mantle melilites. We would not necessarily expect to see a correlation between the minor element content of the spinels correlated with their host $X_{Åk}$ values if they were relics.

The Edge 3 grains in TS-34 are perhaps the best candidates for relict grains in that they show a unique correlation between Cr and V that is observed in no other place (Fig. 3). These could represent a crystallization trend of spinels from a previous generation of igneous CAIs.

SUMMARY

A major goal of science is to resolve alternative interpretations, but perhaps somewhat embarassingly, our conclusion is all of the above.

Modeling of the (Ti, V) trends for spinel inclusions in clinopyroxene (Appendix A) has only moderate success, and even then can only account for the centers of gravity of the observed trends. The general conclusion from the modeling that most spinel inclusions in clinopyroxene should have low Ti conflicts with observation. The V trends cannot be reproduced with simple Constant D and Modal Crystallization models. In contrast, the overall systematics for clinopyroxene inclusions can be explained more easily by subsolidus re-equilibration. The overall scatter can be explained by both hypotheses, although the lack of consistent zoning trends can be explained better by re-melting than by re-equilibration. However, to us, the arguments for the origin of the (Ti, V) trends for spinel inclusions in clinopyroxene by local subsolidus re-equilibration seem significantly stronger.

In contrast, the large Ti and V variations for spinel inclusions in melilite are best explained by the re-melting hypothesis. The (Ti, V) trends for spinel inclusions in the core melilite (Figs. 1c, 5, 7, and 8) probably do primarily reflect recrystallization of spinel after re-melting with some, perhaps chaotic, overprint due to partial re-equilibration involving changes in V concentrations of the order of 0.1% or less.

Our data also show that no relationship exists between the oxygen isotopic compositions of spinels with those of their host silicates. Nor is there any relationship between minor element concentrations and oxygen isotopes. The implication of our finding is that oxygen isotope exchange within silicates occurred after re-melting of the object and/or the exchange event(s) was not the same as that which altered the minor elements' abundance within spinels.

Acknowledgments–We thank J. R. Beckett for numerous discussions and helpful comments that vastly improved this manuscript. We also thank A. El Goresy, S. Simon, L.

Grossman, S. Russell, and G. MacPherson for helpful discussions. We are grateful to L. Grossman for the loan of Allende TS-34 and the Smithsonian for the loan of Leoville 3537-–2. We thank A. Davis, H. Yurimoto, an anonymous reviewer, D. Mittlefehldt, and H. Nagahara for constructive and helpful comments. This research was funded by NASA NAG5–4319, D. S. Burnett PI and NASA NAG5–9789, K. D. McKeegan PI. The UCLA ion microprobe facility is partially supported by a grant from the NSF Instrumentation and Facilities program.

REFERENCES

Beckett J. R. 1986. The origins of calcium-aluminum-rich inclusions from carbonaceous chondrites: An experimental study. Ph.D. dissertation, University of Chicago, Chicago, Illinois, USA. pp. 373.

Beckett J. R., Spivack A. J., Hutcheon I. D., Wasserburg G. J., and Stolper E. D. 1990. Crystal chemical effects on the partitioning of trace elements between mineral and melt: An experimental study of melilite with applications to refractory inclusions from carbonaceous chondrites. *Geochimica et Cosmochimica Acta* 54: 1755–1774.

Beckett J. R., Simon S. B., and Stolper E. 2000. The partitioning of Na between melilite and liquid: Part II. Applications to Type B inclusions from carbonaceous chondrites. *Geochimica et Cosmochimica Acta* 64:2519–2534.

Clayton R. N. 1993. Oxygen isotopes in meteorites. *Annual Review of Earth and Planetary Sciences* 21:115–149.

Clayton R. N., Onuma N., Grossman L., and Mayeda T. K. 1977. Distribution of the pre-solar component in Allende and other carbonaceous chondrites. *Earth and Planetary Science Letters* 34:209–224.

Connolly H. C. Jr. and Burnett D. S. 1999. A study of the minor element concentrations of spinels from two type B calcium-aluminum-rich inclusions: An investigation into potential formation conditions of calcium-aluminum-rich inclusions. *Meteoritics & Planetary Science* 34:829–848.

Connolly H. C. Jr. and Burnett D. S. 2000. The re-melting of type B CAIs: Relationship between the minor element concentrations in spinel to their host silicate (abstract #1440). 31st Lunar and Planetary Science Conference. CD-ROM.

Connolly H. C. Jr. and Burnett D. S. 2001. Experimental constraints on type B CAI formation: Spinel minor elements (abstract #1149). 32nd Lunar and Planetary Science Conference. CD-ROM.

Connolly H. C. Jr. and Love S. G. 1997. The formation of chondrules: Petrologic tests of the shock wave model. *Science* 280:62–67.

Davis A. M., Simon S. B., and Grossman L. 1992. Melilite composition trends during crystallization of Allende Type B1 refractory inclusion melts (abstract). 23rd Lunar and Planetary Science Conference. pp. 281–282.

Davis A. M. and MacPherson G. J. 1996. Thermal processing in the solar nebula: Constraints from refractory inclusions. In *Chondrules and the protoplanetary disk*, edited by Hewins R. H., Jones R. H., and Scott E. R. D. Cambridge: Cambridge University Press. pp. 71–76.

Davis A. M., Simon S. B., and Grossman L. 1998. Reexamination of the Allende type B1 CAI NMNH 5241 (abstract #1948). 29th Lunar and Planetary Science Conference. CD-ROM.

Jones R. H., Lee T., Connolly Jr. H. C., Love S. G., and Shang H. 2002. Formation of chondrules and CAIs: Theory vs. observation. In *Protostars and planets IV*, edited by Mannings V., Boss A. P., and Russell S. S. Tucson: University of Arizona Press. pp. 927–962.

Johnson M. L., Burnett D.S., and Woolum D.S. 1988. Relict refractory element rich phases in Type B CAI. *Meteoritics* 23:276.

Lin Y. and Kimura M. 2000. Two unusual type B refractory inclusions in the Ningqiang carbonaceous chondrite: Evidence for relict, xenoliths, and multi-heating. *Geochimica et Cosmochimica Acta* 64:4031–4047.

MacPherson G. J. and Davis A. M. 1993. A petrologic and ion microprobe study of a Vigarano type B refractory inclusion: Evolution by multiple stages of alteration and re-melting. *Geochimica et Cosmochimica Acta* 57:231–243.

MacPherson G. J., Wark D. A., and Armstrong J. T. 1988. Primitive material surviving in chondrites: Refractory inclusions. In *Meteorites and the early solar system*, edited by Kerridge J. F. and Matthews M. S. Tucson: University of Arizona Press. pp. 746–807.

McKeegan K. D. and Leshin L. A. 2001. Stable isotope variations in extraterrestrial materials. In *Stable Isotope geochemistry, reviews in mineralogy & geochemistry.* Vol. 43. Edited by Valley J. W. and Cole D. R. The Mineralogical Society of America. pp. 279–318.

McKeegan K. D., Leshin L. A., Russell S. S., and MacPherson G. J. 1998. Oxygen isotopic abundances in calcium-aluminum-rich inclusions from ordinary chondrites: Implications for nebular heterogeneity. *Science* 280:414–418.

Meeker G. P., Wasserburg G. J., and Armstrong J. T. 1983. Replacement textures in CAI and implications regarding planetary metamorphism. *Geochimica et Cosmochimica Acta* 47: 707–721.

Ryerson F. J. and McKeegan K. D. 1994. Determination of oxygen self-diffusion in åkermanite, anorthite, diopside, and spinel: Implications for oxygen isotopic anomalies and the thermal histories of Ca-Al-rich inclusions. *Geochimica et Cosmochimica Acta* 58:3713–3734.

Simon S. B., Davis A. M., Richter F. M., and Grossman L. 1996. Experimental investigation of the effect of cooling rate on melilite/liquid distribution coefficients for Sr, Ba, and Ti in type B refractory inclusion melts (abstract). 27th Lunar and Planet Science Conference. pp. 1201–1202.

Simon S. B., Grossman L., and Davis A. M. 1991. Clinopyroxene composition trends during crystallization of Allende Type B refractory inclusion melts. *Geochimica et Cosmochimica Acta* 55:2635–2655.

Simon S. B., Kuehner S. M., Davis A. M., Grossman L., Johnson M. L., and Burnett D. S. 1994. Experimental studies of trace element partitioning in Ca-Al-rich compositions: Anorthite and perovskite. *Geochimica et Cosmochimica Acta* 58:1507–1508.

Simon S. B., McKeegan K. D., Ebel D. S., and Grossman L. 2000. Complexly zoned Cr-Al spinel found in situ in the Allende meteorite. *Meteoritics & Planetary Science* 35:215–228.

Slodzian G., Chainteau M. P., and Dennebouy R. C. 1987. SIMS: Self-regulated potential at insulating surfaces in presence of a strong electrostatic extraction field. *CAMECA News*. pp. 1–6.

Stolper E. 1982. Crystallization sequence of Ca-Al-rich inclusions from Allende: An experimental study. *Geochimica et Cosmochimica Acta* 46:2159–2180.

Stolper E. and Paque J. 1986. Crystallization sequences of Ca-Al-rich inclusions from Allende: The effects of cooling rate and maximum temperature. *Geochimica Cosmochimica Acta* 50: 1785–1806.

Young E. D. and Russell S. S. 1998. Oxygen reservoirs in the early solar nebula inferred from an Allende CAI. *Science* 282:452–455.

Yurimoto H., Ito M., and Nagasawa H. 1998. Oxygen isotope exchange between refractory inclusion in Allende and solar nebula gas. *Science* 282:1874–1877.

APPENDIX

Modeling Spinel Ti Variations During Clinopyroxene Crystallization

Quantitative modeling can test the hypothesis that the observed Ti variations in spinel and clinopyroxene represent crystallization following remelting, thus subsolidus re-equilibration is negligible. Such modeling is conceivable because type B1 CAIs have been intensively studied. However, enough knowledge gaps remain that we are required to fit the observed trends as opposed to making completely independent predictions.

The problem is to model the fractional crystallization of the liquid produced by partial remelting. We assume that the core of the original CAI melted, dissolving all clinopyroxene and anorthite as well as all of the spinel and melilite in the core. We model a three-stage crystallization sequence suggested by the Ti-V systematics (see text): Stage I. Co-crystallization of spinel and clinopyroxene until a fraction crystallized, F_m, where melilite appears. F refers to the fraction of the liquid produced by remelting. Stage II. Crystallization of melilite, spinel, and clinopyroxene until Stage III where anorthite appears at $F = F_a$. We assume that F_a is greater than 90% and only model stages I and II, ignoring anorthite. For type B CAIs in general, the variation of Ti and V concentrations in the liquid is controlled by clinopyroxene crystallization. Minor element concentrations in spinel crystallizing at any amount crystallized are calculated based on the liquid Ti and V concentrations and adopted spinel partition coefficients. As anticipated in proposing the model, Ti and V are compatible elements in clinopyroxene. Thus, Ti and V concentrations in co-crystallizing spinel and clinopyroxene will decrease with increasing crystallization, qualitatively accounting for the observed trends. We assume interface equilibrium (no liquid boundary layers) and modal crystallization, i.e., the relative proportions of phases are assumed constant. We also assume that all spinel inclusions in clinopyroxene were crystallized from the liquid following remelting and that a spinel inclusion co-crystallized with the clinopyroxene adjacent to it. These assumptions, particularly the latter, can easily be violated.

We initially focus on Ti because sufficient data exist to treat Ti^{+3} and Ti^{+4} separately. It is likely that the V variations require separate treatment of V^{+2} and V^{+3} crystallization, and possibly other valence states. But, this has considerable more uncertainties, as discussed below. It is well established that clinopyroxene Ti^{+3}/Ti^{+4} is variable (e.g. Beckett 1986, Simon, Grossman, and Davis 1991). There are a variety of possible reasons for this variability, but it makes plausible the assumption that Ti valence state re-equilibration in the liquid with an external gas phase did not occur during clinopyroxene crystallization. Thus, we assume that Ti^{+3} and Ti^{+4} can be treated as independent elements.

Two semi-independent approaches have been used:

A. Mass balance model, based on Ti^{+3} and Ti^{+4} clinopyroxene zoning profiles. Following Simon et al. (1994), measured Ti^{+3} and Ti^{+4} clinopyroxene zoning profiles are assumed to give concentrations as a function of fraction clinopyroxene crystallized, f_p:

$$f_p = (r/R)^3 \quad \text{(A1)}$$

where r is the distance from the center of the clinopyroxene crystal to a point along a direction for which the center-edge distance is R. Since r and R are known for a given profile, an f_p can be associated with measured Ti concentrations. This assumes uniform growth with a constant crystal shape at all stages in the growth, which may be questionable. The advantage of this approach is that it is not necessary to adopt or infer Ti crystal/liquid clinopyroxene partition coefficients.

B. Constant D model, in which the maximum observed clinopyroxene Ti^{+3} and Ti^{+4} concentrations are assumed to represent the first clinopyroxene crystallized. With an independent estimate of the remelted liquid composition, partition coefficients (D_3[cpx] and D_4[cpx]) can be calculated from which the remaining fractional crystallization can be modeled.

Mass Balance Model

Sectioning effects will tend to flatten an observed zoning profile compared to ones that go through the actual crystal core. Consequently, as opposed to an average zoning profile as used by Simon et al. (1994), we have adopted the steepest measured clinopyroxene profile for TS-34, that given in Fig. 5 of Simon, Grossman, and Davis (1991). Using equation A1, the observed Ti^{+3} and total Ti profiles were replotted as f_p profiles and, following Simon et al. (1994), the concentration profiles C were fit with a 3rd degree polynomial:

$$C = a + bf_p^{1/3} + cf_p^{2/3} + df_p$$

The Ti^{+3} and total Ti profiles were used because these are more precise than those of Ti^{+4}, which is typically 1/3 to 1/4 as abundant as Ti^{+3}. During the modeling, Ti^{+4} concentrations were calculated as the difference between total Ti and Ti^{+3}.

Based on the melilite Na profiles of Beckett et al (2000) and our spinel Ti-V systematics, the remelting of TS-34 appears to have involved the core and part of the mantle melilite. For TS-34, modal mineralogy and bulk composition are available from Beckett (1986) who estimates the core to be 48% by volume. This is probably a lower limit on the amount melted, although there are some core melilites with low Ak (Beckett, private communication). In the remelting, we assume that all clinopyroxene and anorthite is dissolved, along with all of the spinel in the inclusion core. We specifically assume that about 80% of the spinel is dissolved, based on the fraction of spinel in the core of TS-34 measured by Beckett (1986). This corresponds to a clinopyroxene/

spinel ratio of 3:1 after crystallization of the remelted liquid, but results are insensitive to this choice.

The zoning profile equations define average clinopyroxene Ti^{+3} and total Ti concentrations. With modal clinopyroxene abundance from Beckett (1986), the initial liquid concentrations are essentially defined:

$$[Ti^{+3}]ol \cong <Ti^{+3}>_{cpx} F_p \quad (A2)$$

where the [ ]ol brackets refer to weight concentration in the original liquid following remelting, < > refers to average clinopyroxene weight concentration, and F_p is the mass fraction of clinopyroxene after crystallization of the liquid produced by remelting:

$$F_p = (\text{bulk modal clinopyroxene})/M \quad (A3)$$

where the bulk modal clinopyroxene (25% for TS-34) is from Beckett (1986) and M is the fraction of the original inclusion remelted. There are similar equations for the total Ti. Equation A2 is not exact because small amounts of Ti are present in spinel and melilite.

Spinel partition coefficient estimates are guided by preliminary data from Connolly and Burnett (2001) for the C-CO buffer, comparable to that expected for solar nebula conditions. However, the proportions of tri- and tetravalent Ti in the experiments are unknown. Similarly, precise knowledge of the oxygen fugacity appropriate to the TS-34 remelting event is also lacking. Consequently, the partition coefficient for Ti^{+3} in spinel, D_3(sp), has to be regarded as an adjustable parameter. However, the spinel partition coefficient for Ti^{+4} (0.04) is reasonably well-defined by experiments at high oxygen fugacity.

The appearance of melilite at $F = F_m$ is calculated by the point in the crystallization at which the spinel Ti concentration equals the maximum value observed in spinel inclusions in core melilite which we take as 0.25% for TS-34. Overall, results are not critically dependent on this choice. Since F_m is determined by the data being described, this calculation is a fit rather than a prediction. Nevertheless, as illustrated in Table A1 the Material Balance model has the advantage that there are only two adjustable parameters: the partition coefficient of Ti^{+3} in spinel, D_3(sp), and the fraction remelted, M. However, as discussed above, M is restricted to a relatively small range. Consequently, as given in Table A1, we are able to define a "baseline" set of fit parameters based on independent information. The baseline value of D_3(sp) = 0.2 is the total D_{Ti}(sp) measured at the C-CO buffer by Connolly and Burnett (2001). The bulk Ti^{+3} and total Ti concentrations in Table A1, derived from the clinopyroxene zoning profiles, are in acceptable agreement with those from the modal analyses of Beckett (1986): $Ti^{+3} = 0.7 \pm 0.3\%$ and total $Ti = 1.2 \pm 0.4\%$.

The mass balance calculation of the crystallization of the liquid produced by remelting was done numerically on a spread sheet, beginning with steps of 0.2% crystallization to follow the initial rapid decrease of Ti^{+3} concentration in the clinopyroxene, but after 1% crystallization, coarser steps of 1% crystallization were used. The Ti^{+3} and Ti^{+4} distributions were followed separately. The calculation was iterated to account accurately for the amounts of Ti^{+3} and Ti^{+4} in spinel and melilite. This step is important to obtain an internally consistent solution for high degrees of crystallization. Values for Ti^{+3} and Ti^{+4} partition coefficients in melilite (D_3[mel] = 0.02 and D_4[mel] = 0.01) are adopted based on unpublished data. Within each of the stages, we assume that the proportions of the different phases are constant (i.e., modal crystallization), an assumption that could be significantly in error.

The baseline model is an instant failure in that, with D_3(sp) = 0.2, the calculated maximum spinel Ti concentrations at the beginning of crystallization are only about 0.22–0.24%, far less than observed (around 0.7%). To match 0.7% spinel Ti with D_3(sp) = 0.2, the required fraction melted is only 20–25%, which seems unreasonably small.

However, as discussed above, we can legitimately regard D_3(sp) as an adjustable parameter, and for a value of 0.52, the resulting calculated profile is shown in Fig. A1. Fit parameters (set D) are shown in Table A1. All models assume that co-crystallized spinel and clinopyroxene are not physically separated, an assumption that may not be true in practice. In any case, the significant scatter in the TS-34 data makes these a relatively soft target for fitting. Varying the fraction of inclusion remelted over the range 40 to 65% gives equivalent fits but always with D_3(sp) in the range of 0.5. The kink in the calculated curve reflects the appearance of melilite

Table A1. TS-34 Mass balance parameters.

Fixed parameters	Baseline set	
Bulk modal abundances (wt%)[a]		
clinopyroxene	25	
spinel	10	
melilite	64	
anorthite	1	
$<Ti^{+3}>$cpx	2.64%	
<Titotal >cpx	3.55	
Recrystallized clinopyroxene/spinel	3.1	
D_4 (sp)	0.04	
D_3 (mel)	0.02	
D_4 (mel)	0.01	
i (sp) at $F = F_m$[b]	0.25%	
Variable parameters	Baseline set	Set D
Bulk Ti^{+3}	0.66%[c]	0.69%
Bulk total Ti	0.89%[c]	0.92%
Fraction remelted[d]	60%	60%
D_3 (sp)	0.2	0.52

[a]Beckett (1986).
[b]Spinel Ti concentration at time of melilite appearance.
[c]Clinopyroxene contribution; fixed. Total varied slightly to match uptake by spinel and melilite.
[d]Allowed to vary: 50–65%.

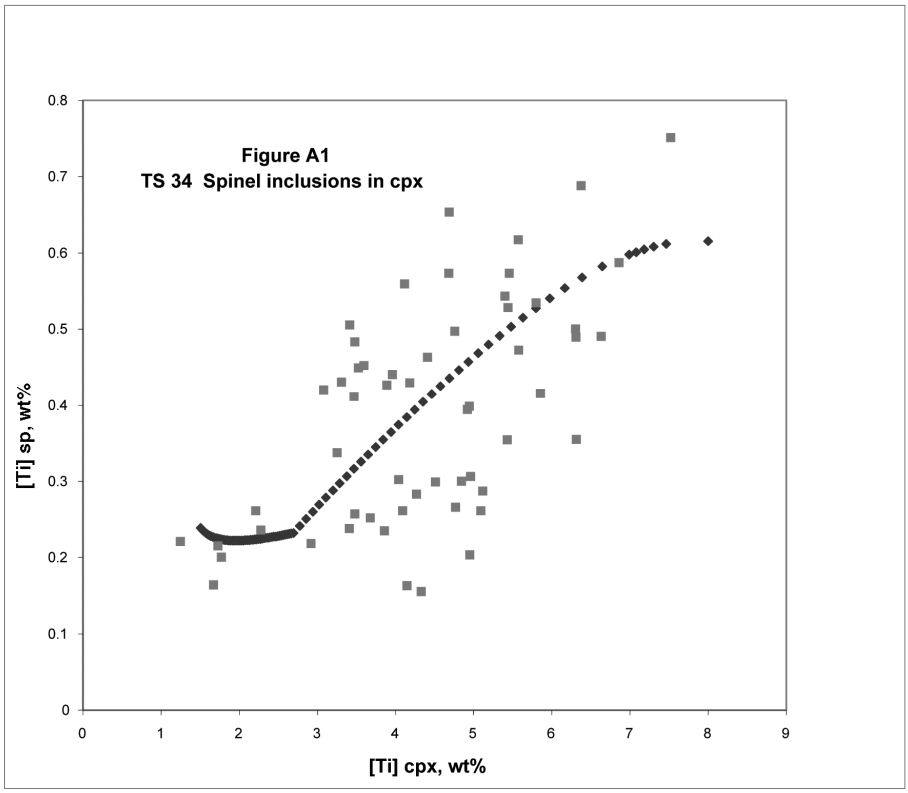

Fig. A1. Comparison of predictions of mass balance model for spinel inclusions in TS-34 clinopyroxene compared with measured Ti concentrations in spinel and clinopyroxene. See Table A1 for parameters. The calculated curve in Figure A1 is terminated at F = 0.85. The first crystallizing spinels have the highest Ti concentrations. Below about 7% Ti in clinopyroxene each point on the calculated trend corresponds to 1% crystallization. Just below 3% Ti in clinopyroxene, melilite appears (36% crystallization). For larger amounts of crystallization, the liquid Ti concentration varies, slowly halting the decrease in spinel Ti concentrations. The analyses all refer to small (15–30 micron) spinel grains. The model assumes that the spinels are incorporated as inclusions in clinopyroxene as fast as they are formed. Most spinel inclusions in clinopyroxene should have low Ti concentrations, but this is not observed.

at $F_m = 0.36$. At high F, the amounts of both Ti^{+3} and Ti^{+4} removed from the liquid by clinopyroxene in a given crystallization step are less. This is because, with essentially Ti-free melilite accounting for a significant fraction of the crystallization (67% for parameter set D), the liquid and thus the spinel Ti concentrations stop falling and actually begin to rise in the latter stages of crystallization. With better-defined observed trends, the presence or absence of a kink might be a definitive test of the validity of the remelting model, but this is not possible, given the amount of scatter in the actual data.

Constant D Model for TS-34

This model is less constrained, but a priori no less valid, than the material balance model. The Constant D model can also be applied to the data for spinel inclusions in clinopyroxene from Leoville 3537–2 for which the relevant trends have less scatter. For TS-34, in order to improve physical insight, we vary the fraction melted, M, and the bulk Ti^{+3} and Ti^{+4} concentrations, although the results depend only on the concentrations in the liquid after remelting:

$$Ti^{+3}_{l0} = \text{bulk } Ti^{+3}/M \quad \text{(A4)}$$

where Ti^{+3}_{l0} is the initial Ti^{+3} concentration in the liquid after melting. An analogous equation can be written for Ti^{+4}. Equation A4 assumes that negligible Ti is in the unmelted fraction, which is a good assumption.

For TS-34, we can carry over the bulk modal abundances, D_4(sp), and the melilite partition coefficients as fixed parameters from the mass balance model. We calculate the required Ti^{+3} and Ti^{+4} clinopyroxene partition coefficients (D_3[cpx] and D_4[cpx]) from the model initial liquid concentrations (Equation A4) and the observed maximum (i.e., initial) Ti^{+3} or Ti^{+4} concentrations in clinopyroxene:

$$D_3(\text{cpx}) = (\text{max } Ti^{+3} \text{ in cpx})/Ti^{+3}_{ol} \quad \text{(A5)}$$

with an analogous equation for Ti^{+4}. A standard fractional crystallization calculation gives the liquid Ti^{+3} and Ti^{+4} concentrations as a function of fraction crystallized (F). Predicted Ti concentrations in spinel co-crystallizing with clinopyroxene follow from the adopted spinel partition coefficients. As with the mass balance model, melilite is

assumed to appear when the spinel Ti concentration matches the observed maximum Ti concentration for spinel inclusions in core melilite (0.25%). All partition coefficients are assumed constant, although this may not be true.

For TS-34, we can define a set of baseline parameters, analogous to that done for the mass balance model (Table A2). However, the baseline parameters fail in the same way as for the mass balance model in that the first formed spinels are predicted to have Ti contents of 0.28%, much lower than observed. Even if we vary the fraction melted or, equivalently, the bulk abundances, it is not possible to describe the data with D_3(sp) less than about 0.4.

Fig. A2 shows that an apparently reasonable description of the data for spinel inclusions in clinopyroxene can be obtained by appropriate variation of parameters (Set K; Table A2). Except for the increase in D_3(sp), the parameters in set K are similar to the baseline. $F_m = 34\%$ for the model on Fig. A2. The values of bulk Ti^{+3} and Ti in Table A2 should be regarded as illustrative. Given the scatter of the data, fine tuning of these parameters is not justified. The values of bulk Ti^{+3} and Ti are within the uncertainty range quoted by Beckett (1986).

Table A2. Parameters for constant D models of TS-34.[a]

Fixed parameters	Baseline	
max Ti^{+3} (cpx)	6.5%	
max Ti^{+4} (cpx)	1.6%	
D_4 (sp)	0.04	
D_3 (mel)	0.02	
D_4 (mel)	0.01	
Ti (sp) at F = F_m[b]	0.25%	
Variable parameters	Baseline	Set K
fraction melted	60%	60%
bulk Ti^{+3}[c]	0.7[c]	0.88
bulk Ti[c]	1.2[c]	1.08
D_3 (sp)	0.2	0.45
D_3 (cpx)[d]	5.6	4.4
D_4 (cpx)[d]	1.9	4.8

[a]Bulk modal abundances as in Table A1.
[b]Spinel Ti concentration at time of melilite appearance.
[c]Beckett (1986).
[d]These are determined once the bulk Ti^{+3} and Ti are specified.

Table A3. Parameters for constant D models of Leoville 3537–2.

Fixed parameters	
max Ti^{+3} (cpx)	4.0%
max Ti^{+4} (cpx)	1.3%
D_4 (sp)	0.04
D_3 (mel)	0.02
D_4 (mel)	0.01
T (sp) at F = F_m[a]	0.18
Variable parameters	Set F
modal abundances[b]	
clinopyroxene	0.45
spinel	0.15
melilite	0.40
$Ti^{+3}{}_{l0}$[c]	0.90%
$Ti^{+4}{}_{l0}$[c]	0.27%
D_3 (sp)	0.45
D_3 (cpx)	4.4
D_4 (cpx)	3.6

[a]Spinel Ti concentration at time of melilite appearance.
[b]Entries refer to weight fractions of phases produced by crystallization of the liquid after remelting.
[c]Concentrations in liquid produced by remelting.

Constant D Model for Leoville 3537–2

The detailed modal mineralogical data available for TS-34 is lacking for Leoville 3537–2. Thus, specification of a baseline set of parameters is not possible. We do have sufficient data to define maximum (i.e., initial) Ti^{+3} and Ti^{+4} clinopyroxene concentrations (Table A3). The Leoville data introduce a significant constraint in that the overall Ti concentrations are lower. But for this remelting model to be valid, we are required to have a consistent solution between the TS-34 and Leoville 3537–2 data such that the same pyroxene and spinel partition coefficients describe both sets of data. The oxygen fugacities may not have been the same for the two CAIs, but assuming that Ti^{+3} and Ti^{+4} partition as separate elements in both, the partition coefficients for a specific valence state should be similar, neglecting any effect of bulk compositional differences on the partition coefficients.

Fig. A3 shows a fit to the Leoville Ti data for the parameters given in Table A3. Note that Ti concentrations in Table A3 refer to the liquid produced by remelting and cannot be compared directly with the bulk Ti concentrations in Table A2. In general, all Ti concentrations are lower than for TS-34, but a respectable description of the Leoville data can be obtained using the same clinopyroxene and spinel partition coefficients as for TS-34 (Table A2). The remelting hypothesis is a success in this respect.

In selecting acceptable solutions, particular care was taken to fit the full range of clinopyroxene Ti concentrations. This requires keeping the Ti bulk partition coefficients, particularly for Ti^{+3}, sufficiently large that the liquid Ti concentrations continue to drop after melilite appearance. The fits shown in Figs. A2 and A3 meet this constraint.

Ti Modeling: Discussion and Comparisons

A model consequence that is conceivably fatal to the remelting hypothesis is that, for all of the above models, most (64, 66, and 71% for Figs. A1, A2, and A3) of the crystallization occurs after melilite appearance. Thus, most of the spinel inclusions in clinopyroxene should have relatively low Ti contents, contrary to what is observed in both Leoville and TS-34. This is a general feature of all parameter sets which describe the data, even if solutions are forced for a high value of F_m, in which a large fraction of spinel has crystallized prior to melilite appearance. In these cases, the spinel Ti

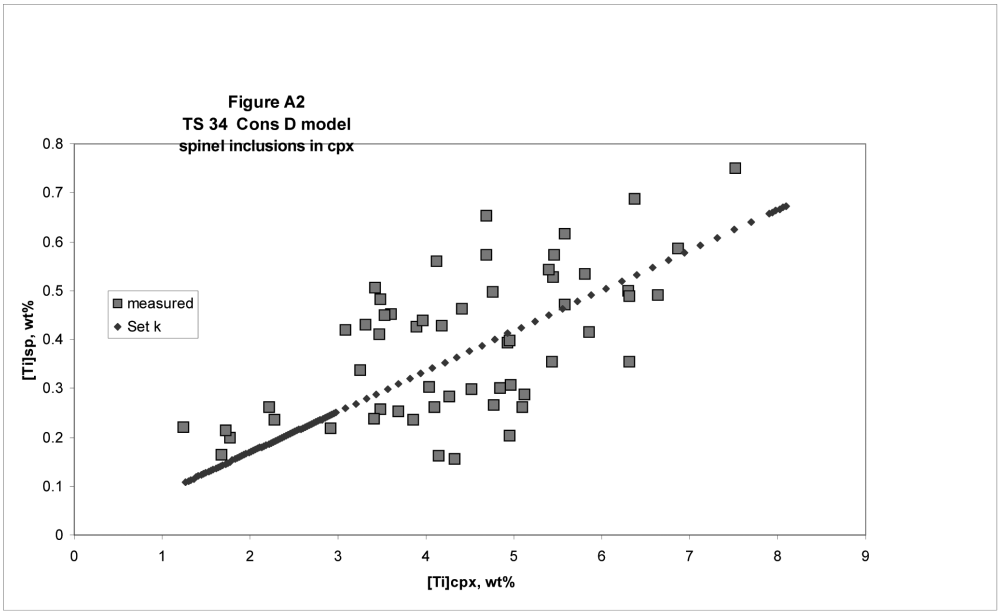

Fig. A2. Comparison of predictions of the constant D model for spinel inclusions in TS-34 clinopyroxene compared with measured Ti concentrations in spinel and clinopyroxene. See Table A2 for parameters. The first crystallizing spinels have the highest Ti concentrations. Just below 3% Ti in clinopyroxene, melilite appears (34% crystallization). For larger amounts of crystallization, the liquid Ti concentration varies, slowly producing a decrease in spinel Ti concentrations. Most spinel inclusions in clinopyroxene should have low Ti concentrations, but this is not observed.

concentrations decrease rapidly, and most spinels still have relatively low Ti.

This potential failure mode could be mitigated if the modal crystallization hypothesis is wrong and if spinel crystallization (or nucleation) stops early, e.g., shortly after melilite appearance. Then, most spinels might have high Ti concentrations. Cessation of spinel crystallization is observed in laboratory experiments on bulk CAI compositions. If spinel crystallization did stop early, there should be no correlation of Ti or V concentrations for spinel inclusions in melilite with melilite $X_{Åk}$. Such correlations may or may not be present (Figs. 5–7). However, if spinel crystallization stopped early and the spinel inclusions in core melilites just represented those that were not incorporated into clinopyroxene, then the same compositional ranges should be seen in clinopyroxene inclusions and in core melilite inclusions, which is not true. We conclude that the small observed fraction of low Ti spinel inclusions in clinopyroxene is a serious problem for the remelting hypothesis.

It is far from obvious that the best fit should be to the center of gravity of the data, as has been done for Figs. A1–A3. The appropriate fit depends on understanding the source of the significant scatter in the data for the spinel inclusions in clinopyroxene. The most obvious mechanism for scatter is for spinel inclusions formed at a fraction crystallized F_1 to be captured as an inclusion at a later time F_2, so that the Ti concentrations for these spinels are too high relative to trends for co-crystallizing spinel and clinopyroxene for the clinopyroxene Ti where it was included. From this point of view, the trend for co-crystallizing spinel and clinopyroxene is defined by the "lower boundary" of the field of data points, i.e., the boundary on the high clinopyroxene Ti and low spinel Ti sides. Although this lower boundary is not well defined in the data, even for TS-34 where a large number of analyses are available, it appears to be characterized by a high degree of curvature, initially rapidly dropping spinel Ti compared to clinopyroxene Ti, but becoming the opposite (approximately constant spinel Ti over a wide range of clinopyroxene Ti) for higher degrees of crystallization. It is not possible to produce trends with this type of curvature in either of the above models. The mass balance co-crystallization trends have the opposite curvature, and the constant D model tends to produce approximately linear trends. Either this interpretation for the scatter is incorrect, the assumption of constant D is seriously in error, or the trends for spinel inclusions in clinopyroxene were not produced during crystallization of the remelted liquid.

V Modeling

As indicated above, we believe that it is necessary to model the V partitioning of V^{+3} and V^{+2} separately. But, as we might be wrong, we tested constant D models for the V data for both TS-34 and Leoville 3537–2, using the successful Ti fits from Figs. A2 and A3. However, even allowing no constraints on the V partition coefficients and the V content of the liquid produced by remelting, no reasonable descriptions of the data were obtained. The impossible challenge was to

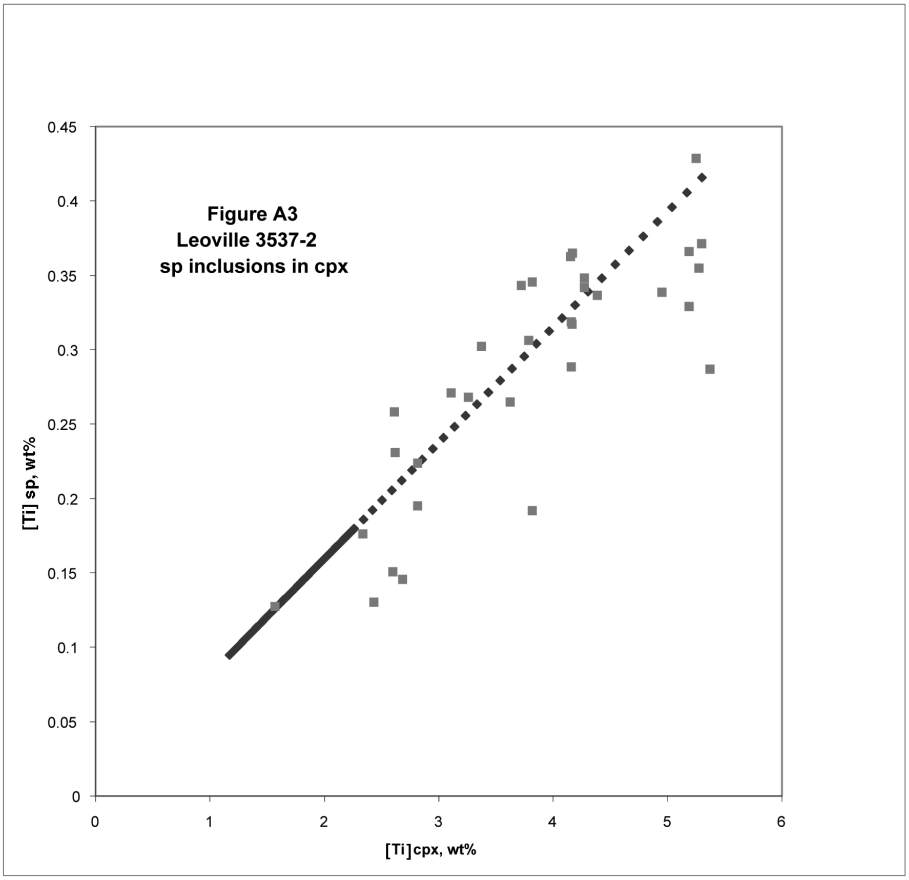

Fig. A3. Comparison of predictions of the Constant D model for spinel inclusions in Leoville 3537–2 clinopyroxene compared with measured Ti concentrations in spinel and clinopyroxene. See Table A3 for parameters. The model is successful in describing both TS-34 and Leoville with the same adopted spinel and clinopyroxene Ti crystal-liquid partition coefficients. In this model, melilite appears around 2.3% Ti in clinopyroxene (29% crystallization) and the liquid, spinel, and clinopyroxene concentrations vary slowly after this. Most spinel inclusions in clinopyroxene should have low Ti concentrations, but this is not observed.

model the relatively flat slope of the spinel V versus clinopyroxene V for spinel inclusions in clinopyroxene (Figs. 8 and 9), which can be explained by the subsolidus re-equilibration hypothesis (see text).

It appears possible that the V trends are potential discriminators between the subsolidus re-equilibration and remelting hypotheses. Thus, although a priori ludicrous, we have explored whether there is any set of parameters in a V^{+3} and V^{+2} crystallization model that can describe the data. We refer to this as the "V2" model. Now, we have 6 parameters to vary. Surely, something can be made to work. However, it turns out to be difficult, again because of the flat slope of the spinel V versus clinopyroxene V trend. We restrict discussion to the Leoville data, which have considerably less scatter. A reasonable description of the V data can be obtained if we let V^{+2} be highly compatible in spinel (D_{V2}(sp) = 7–8). However, we consider this totally unreasonable. Another possible solution is to assume that V^{+2} is moderately compatible in melilite (D_2(mel) ≅ 1) and that the initial V^{+2}/V^{+3} is high (about 2). However, this model predicts melilite V concentrations in the 0.1–0.2 range, in total disagreement even with the 0.01% upper limit from our electron probe analysis.

We have found no fractional crystallization model that can describe the V trends on Figure 9.

Overall, our models could be too simplistic in assuming constant partition coefficients, modal crystallization, etc. But taking the above failures at face value, a re-equilibration origin for the (Ti, V) trends for spinel inclusions in clinopyroxene is preferred.

It has been suggested that our failure to model the observed trends for spinel inclusions in clinopyroxene might be explained by the failure of the interface equilibrium assumption. Since disequilibrium effects are difficult to model, this can never be completely ruled out. Nevertheless, regarding V as a moderately compatible element, ubiquitous and severe boundary layer effects would cause all measured V concentrations to be low. Likewise, as a moderately incompatible element, all measured Ti concentrations would be high. If boundary layer effects were dominant, then V zoning profiles in spinel should always show core enrichments and Ti zoning profiles should always show core depletions. These predictions are contrary to observations.